Contrib Mineral Petrol (1983) 84:152–173

Contributions to Mineralogy and Petrology

Trace element abundances and mineral/melt distribution coefficients in phonolites from the Laacher See Volcano (Germany)

G. Wörner[1], J.-M. Beusen[2], N. Duchateau[2], R. Gijbels[2], and H.-U. Schmincke[1]
[1] Institut für Mineralogie, Ruhr Universität Bochum, Postfach 102148, D-463 Bochum, Federal Republic of Germany
[2] University of Antwerp (U.I.A.), Department of Chemistry, B-2610 Wilrijk, Belgium

Abstract. Twenty six whole rocks, seven matrix and fifty three mineral separates from the compositionally zoned late Quaternary Laacher See tephra sequence (East Eifel, W-Germany) were analyzed by instrumental neutron activation. These data document the chemical variation within the Laacher See magma chamber prior to eruption with a highly fractionated phonolite at the top and a more mafic phonolite at its base as derived from other data. Incompatible elements such as Zn, Zr, Nb, Hf, U, light and heavy rare earths are extremely enriched towards the top whereas compatible elements (e.g. Sr, Sc, Co, Eu) are strongly depleted. Semicompatible elements (Ta and some middle REE) are depleted at intermediate levels. This chemical variation is shown by whole rock *and* matrix data indicating the phonolite liquid was compositionally zoned regardless of phenocryst content. Hybrid rocks (phonolite-basanite) show the largest concentrations for compatible elements. All elements (except Rb) display continuous compositional variations with regard to the stratigraphic position of pumice samples. From these data we are able to distinguish three main units: An early erupted highly fractionated magma, the main volume of evolved phonolite and a mafic phonolite as the final products.

The extreme variation of trace element distribution coefficients (K) for 9 mineral phases with respect to stratigraphic position (resp. matrix composition) cannot be explained by conventional mechanisms. We postulate a significant modification of the trace element content of the phonolite melt by liquid-liquid controlled differentiation processes subsequent to and/or contemporaneous with (fractional) crystallization which caused disequilibrium between phenocrysts and host matrix. Therefore, our "distribution coefficients" deviate from equilibrium partition coefficients equivalent to the amount of this post crystallization modification of the matrix composition. The relationship between varying K and matrix composition is demonstrated by a ΔK–ΔM-diagram (variation of K versus variation of matrix, M). Different parts of this diagram relate to different parameters (*T*, *P*, polymerization, complex-building, equilibrium crystallization in a zoned magma column and post crystallization disequilibrium effects) which are responsible for the variation of distribution coefficients in general. The ΔK–ΔM-diagram may allow to distinguish between different processes affecting the distribution coefficients measured in natural volcanic rocks from a differentiating magma system.

Offprint requests to: G. Wörner

Introduction

The nature and origin of chemical gradients within high level magma chambers have become a topic of much current interest. Such chemical zonations have been deduced chiefly from zoned pyroclastic deposits especially ash-flow tuffs as reviewed elsewhere in more detail (Smith 1979; Hildreth 1979, 1981; Wörner and Schmincke 1984). Most of these stratified magma chambers studied so far are calcalkaline rhyolitic (Hildreth 1979, 1981; Smith 1979) and andesitic to dacitic compositions (Ritchie 1980). Only few studies have been performed on alkaline rhyolites (Ewart et al. 1968; Schmincke 1969a, b, 1976; Gibson 1970; Mahood 1981). The only investigation on a phonolitic zoned pyroclastic sequence from the Somma-Vesuvius volcano (Barberi et al. 1981) is confined to major element data. Trace elements often allow to specify chemical gradients more vigorously than major elements (see for example Hildreth 1979). Thus, one major purpose of this study is to document the variation of observed trace element abundances in a compositionally zoned phonolite magma chamber. A second aspect concerns the determination of mineral/matrix trace element distribution coefficients and their variations within the stratified magma column.

Distribution coefficients (K) defined as the mass ratio of a given trace element in a solid phase (phenocryst, C_s) and the silicate liquid (C_l):

$$K = C_s/C_l$$

have been reported for a range of natural magma compositions (e.g. Schnetzler and Philpotts 1970; Philpotts and Schnetzler 1970; Nagasawa and Schnetzler 1971). Distribution coefficients determined experimentally in synthetic and natural systems are in reasonable agreement with those found for natural phenocryst/matrix pairs (see Irving 1978 for a review on experimental work on distribution coefficients). However, empirical or experimental studies were performed for basaltic, andesitic to dacitic or rhyolitic whole rock compositions only and data for undersaturated differentiated rocks are rare (Berlin and Henderson 1969; Sun and Hanson 1976; Cullers and Medaris 1977 and Larson 1979 are the only published studies concerned with undersaturated alkaline rocks). Published values of K for a given element and phenocryst phase vary widely depending on host rock compositions and variable physical conditions. These variations are generally believed to be a function of

a) major element composition of the liquid

b) temperature

c) additional parameters such as pressure, mineral composition, trace element concentration, oxygen fugacity and others.

The major element and volatile composition (a) of a magma strongly influences the polymerization of the silicate network of the melt (Watson 1976; Reyerson and Hess 1978; Mahood 1981; Mahood and Hildreth 1983). Temperature dependent partitioning (b) of trace elements between phenocrysts in equilibrium with the matrix were used as geothermometers where calibration was possible (e.g. Häkli and Wright 1967; Hart and Davis 1978; Irving 1978). Factors such as disequilibrium between melt and minerals and the presence of a fluid phase as well as adsorption effects and other physico-chemical complexities may also play a role (Albarede and Bottinga 1972; Dowty 1977; Hanson 1978; and others). Mahood (1981) and Mahood and Hildreth (1983) determined K-values from two large rhyolitic rock suites, which were erupted from compositionally zoned magma chambers. They found strong evidence for the overriding control of melt structure on mineral/melt trace element distribution in one setting (Sierra La Primavera) and irregular trends of distribution coefficients in the other (Bishop Tuff).

The present paper reports trace element data on Laacher See phonolite whole rocks, matrix and mineral separates. Plinian and vulcanian eruptions from the Laacher See volcano 11,000 years ago represent the most recent activity of the Quaternary East Eifel volcanic field, which has been active for the last 0.6–0.7 m.y. (Schmincke and Mertes 1979). During this time, a wide range of potassic mafic and differentiated magmas (basanites, nephelinites, leucitites, tephrites and phonolites) were erupted chiefly in cinder cones and four larger caldera-forming phonolitic centers (Riedener Kessel, Wehrer Kessel, Kempenich volcano and Laacher See volcano). Duda and Schmincke (1978) reviewed the petrography, geochemistry and petrology of the mafic and intermediate suite and a general review of the volcanology and geochemistry of Quaternary Eifel volcanic fields is given by Schmincke (1982) and Schmincke et al. (1983).

The Laacher See pyroclastic sequence, which displays an extreme compositional zonation from early erupted almost phenocryst free, highly differentiated peralkaline phonolite towards a late mafic crystal-rich phonolite shows a strong variation of distribution coefficients (K) for all trace elements and phenocryst phases. Here we concentrate on the presentation of whole rock trace element data and the interpretation of the highly variable distribution coefficients. The compositional zonation within the Laacher See magma chamber is discussed by Wörner and Schmincke (1984).

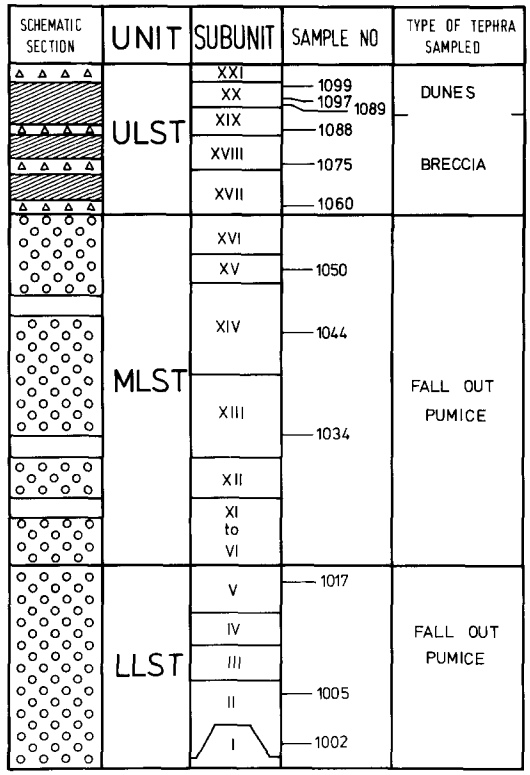

Fig. 1. Highly schematic section of the Laacher See tephra. Three main stratigraphic units (LLST, MLST, ULST = lower, middle, upper Laacher See tephra) as well as 21 subunits are distinguished. LLST is characterized by plinian and phreato-plinian fall out pumice layers, in addition to these, MLST shows intercalated ashflows, and ULST consists of breccia layers, ash-flows and dune beds. The type of tephra sampled for this study is given in the right column. For a full discussion of the Laacher See tephra stratigraphy see Bogaard (1983)

Methods

Sample preparation whole rock samples

Whole rock pumice samples were collected on the basis of the stratigraphic subdivision and correlation between different units of the Laacher See tephra deposits in order to guarantee optimum coverage of the zoned sequence and the compositional variation within a particular tephra layer (sample nos. run in stratigraphic order from 1002 to 1099, Fig. 1). The detailed description of sample localities, stratigraphic relations and type of sampled material is described by Wörner (1982) and Wörner and Schmincke (1984). Each sample was chosen to represent the particular stratigraphic layer it was taken from. Four layers (1060, 1079, 1089, 1097) were selected for multiple sampling to cover the variety of different rock types at these levels. Sample sizes range from 200–400 g for homogeneous, crystal poor pumice (lower stratigraphic units LLST and lower MLST, Fig. 1) to 0.5 to 2 kg for phenocryst-rich (ULST) samples. The material was washed in water, dried at 70° C and carefully crushed (< 2 mm) using a nylon hammer or a nylon coated hydraulic press (dense mafic and hybrid phonolites). Xenolith inclusions, subvolcanic and cumulate fragments were subsequently removed by handpicking under a binocular. Finally, all samples were ground using an agate-disc mill.

Mineral separations

Pumice samples between 1 and 10 kg (porphyritic and glassy samples) were carefully crushed using the nylon hammer or the nylon coated hydraulic press. Some ULST samples had to be desintegrated with a jaw-crusher. Depending on phenocryst size, sieved fractions of the crushed samples (125 to 250 μm and 250 to 500 μm) were washed and separated into matrix and minerals by means of floating in water, heavy liquids and the Frantz magnetic separator. Repeated

separations with frequent treatment in an ultrasonic bath between individual steps were necessary to obtain semi-clean mineral and matrix separates. Luke warm, dilute HF (5%) was used to dissolve glass rims on all minerals except hauyne and apatite. Etching of crystal surfaces is believed to be insignificant judging from optical observations on cleavage faces. Matrix-free mineral separates were then cleaned using the magnetic separator. Handpicking was necessary in order to remove erratic grains, intergrown minerals and inclusions. Further crushing of the minerals, treatment with dilute HF and handpicking finally removed all inclusions in mineral grains. Separated mineral fractions are pure to at least 99% (heavy minerals). Sanidine and plagioclase may be impure with respect to each other and quartz from crushed xenolith inclusions. However, X-ray diffraction patterns of feldspar separates did not show impurities. Therefore, sanidine and plagioclase separates are clean to at least 95–97%. Pure hauyne separates are difficult to obtain due to inevitable glass inclusions and matrix attached to the crystal surface which could not be dissolved with HF. Careful handpicking of clean hauyne crystals, however, removed most impurities resulting in hauyne separates believed to be 99% pure.

Analytical method

The concentrations of Na, K, Sc, Cr, Fe, Co, Zn, Rb, Sr, Zr, Ba, REE (Rare Earth Elements), Hf, Ta, Th and U in whole rocks, matrix and mineral separates of the Laacher See phonolites were obtained by instrumental neutron activation analysis (INAA). The analytical procedures have been described by Hertogen (1974), Hertogen and Gijbels (1971) and Jacobs et al. (1977) and are only briefly summarized here:

Powdered samples ranging from 10 to 600 mg were mixed with appropriate amounts of a high purity wax, homogenized and pressed into pellets. The pelletized samples were transferred into polyethylene capsules and irradiated in the Research Reactor THETIS at the State University of Ghent (Belgium). Selected mineral separates (plagioclase, sanidine, hauyne, phlogopite and some pyroxenes) have also been sealed in ultrapure fused silica tubes following the procedure outlined by Jacobs et al. (1977). These samples were irradiated for 24 h in the Material Testing Reactor BR-2 at Mol (Belgium). Gamma-ray spectra were accumulated using a coaxial 62 cm^3 Ge(Li) detector and a planar 78 mm^2 low energy photon spectrometer. Photopeak interference corrections were made following the procedure described by Hertogen (1974). Errors for INAA are usually less than 10% but vary depending on sample size, concentration and necessity of corrections for spectral interferences (e.g. Ba interference with Nd). Zirconium and holmium results are only precise within 20–50%. The wax used for pelletizing was proven to be very pure so that no blank corrections had to be made.

Results

Twenty six whole rock samples, 53 mineral and 7 matrix separates were analyzed by INAA for trace elements. For most whole rock samples, XRF major and additional trace elements as well as microprobe analyses of all phenocryst phases are also available (Wörner 1982; Wörner and Schmincke 1984). Analytical results are listed in Tables 1 and 2. The stratigraphic subdivision of the Laacher See tephra into three main units (LLST, MLST, ULST: lower, middle and upper Laacher See tephra) is based on earlier

Table 1. Whole rock trace element compositions in ppm (for sample nos – see Wörner (1982) and Wörner and Schmincke (1984)

	ULST							
	1002-1	1002-2	1005-1	1005-2	1005-3	1017-1	1017-2 P.S.[b]	1017-3 P.S.[b]
Na %	8.23	–	–	–	–	–	–	–
Sc	0.15	(1.74)	0.13	0.08	0.11	0.28	0.48	0.19
Cr	2	(21.5)	–	–	–	9.03	–	–
Fe %	1.96	–	–	–	–	–	–	–
Co	0.44	(2.72)	0.46	0.41	0.42	0.91	0.75	0.59
Zn	153	153	131	124	145	97	–	–
Rb	380	295	279	263	292	330	580	564
Sr	3.86[a]	–	–	–	–	35	–	–
Zr	2,200	2,155	1,845	1,845	1,995	1,220	2,460	2,420
Ba	380	425	285	265	350	275	–	–
La	196	196	172	175	203	166	194	185
Ce	304	284	248	243	271	192	247	233
Nd	104	97	92	85	92	44	38	33
Sm	4.31	5.63	3.66	3.87	4.22	3.97	5.20	4.52
Eu	0.48	0.55	0.36	0.39	0.40	0.36	0.51	0.41
Tb	0.54	0.56	0.41	0.38	0.49	0.31	0.39	0.48
Ho	–	–	–	–	–	–	–	–
Yb	7.63	7.31	6.05	6.16	6.90	4.03	6.14	5.76
Lu	1.24	1.16	0.88	1.03	1.09	0.64	1.22	1.15
Hf	41.8	39.5	33.9	34	37.3	20.6	36.6	34.6
Ta	8.16	7.77	6.53	6.56	7.17	4.98	6.93	6.69
Th	115	108	93.7	94.8	104	51.6	92.5	87.5
U	27.5	38.1	31.8	34.3	39.3	21.8	26.3	22.9

[a] Sr by isotope dilution [b] Sample provided by P. Staps

Table 1 (continued)

	MLST				ULST			
	1034	1034-a	1034-2 R.R.[a]	1050	1060-1	1060-2	1060-3	1060-4
Na %	–	–	–	–	4.32	4.70	4.83	4.12
Sc	0.29	1.04	0.22	1.16	1.20	1.41	1.40	1.41
Cr	–	12.1	5	7.1	4	5.1	7.3	4.7
Fe %	–	–	–	–	3.51	4.30	4.09	3.44
Co	0.80	1.99	2.16	2.52	3.04	3.75	3.68	3.35
Zn	62	66	77	–	43	48.8	50.9	41.2
Rb	140	132	247	198	86	88	101	87
Sr	140	161	77	365	1,023	943	1,032	892
Zr	835	830	785	495	359	380	326	402
Ba	185	170	155	325	743	834	766	661
La	114	107	114	90.4	88.9	93.1	90.1	80.1
Ce	159	150	162	143	163	170	161	146
Nd	23	15	34	32	38.3	36.3	41.5	35.8
Sm	3.20	3.34	2.98	4.14	5.95	6.20	5.66	5.64
Eu	0.61	0.63	0.47	1.03	1.88	1.94	1.78	1.71
Tb	0.38	0.39	0.25	0.41	0.56	0.62	0.61	0.56
Ho	–	–	–	–	–	–	–	–
Yb	2.91	3.08	2.87	2.07	2.25	2.21	2.07	2.34
Lu	0.44	0.48	0.46	0.36	0.33	0.33	0.32	0.36
Hf	12.7	12.1	13.3	7.77	6.20	6.52	6.39	6.82
Ta	4.78	4.44	4.61	5.62	7.69	8.07	7.26	6.77
Th	28	26	31.8	15.1	11.3	11.7	12.0	13.0
U	8.2	6.2	10.2	3.87	–	–	–	–

[a] Sample provided by R. Risse

	ULST						Hybrid rocks		1097-2	Representative East Eifel basanite
	1060-5	1079-1	1079-2	1079-3	1079	1088	1089-1	1097-1		Nickenicher Sattel
Na %	4.44	–	–	–	–	–	–	–	–	–
Sc	1.21	1.44	2.69	1.23	1.53	2.16	2.75	2.43	19.4	33.6
Cr	4.5	1.9	8.7	2.1	–	6.5	9	4	120	262
Fe %	3.46	–	–	–	–	–	–	–	–	–
Co	3.28	3.28	5.35	3.42	3.88	4.55	6.7	5.5	22.9	49.5
Zn	41.8	42	49	43	–	41	42	43	–	(90.8)
Rb	88	82	87	79	142	138	66	62	68	85
Sr	798	890	1,125	710	865	1,085	1,251	1,301	982	(709)
Zr	378	310	370	205	325	320	282	204	318	235
Ba	665	335	645	320	720	1,610	1,863	1,764	1,830	(770–879)
La	80.5	73	93	83	85.7	99.2	95.6	85.8	69.6	49.2
Ce	165	140	180	152	163	189	197	177	144	104
Nd	37	28	42	36	53	49	70.5	63	55.3	46.3
Sm	5.86	6.19	8.34	6.17	6.39	8.55	9.5	8.52	8.08	7.86
Eu	1.83	1.73	2.37	1.74	1.90	2.41	2.70	2.42	2.19	2.36
Tb	0.63	0.63	0.78	0.58	0.65	0.92	0.91	0.75	0.75	0.90
Ho	–	–	–	–	–	–	1.01	0.82	0.97	0.79
Yb	2.17	1.94	2.69	2.04	2.41	2.72	2.65	2.28	2.14	1.75
Lu	0.33	0.27	0.39	0.35	0.33	0.40	0.31	0.29	0.35	0.28
Hf	6.64	4.60	5.82	5.13	5.62	5.82	5.32	5.31	5.00	5.97
Ta	7.55	6.33	8.27	5.94	7.83	9.31	9.35	8.19	6.56	4.6
Th	11.50	7.95	10.0	9.61	10.1	10.15	8.97	8.66	7.44	5.70
U	–	3.1	3.1	–	2.67	2.06	1.62	1.96	0.83	1.51

work by Schmincke (1977) and co-workers (for a detailed description see Bogaard 1983).

Trace element variation within the Laacher See tephra sequence

Samples representative for a particular tephra layer (or stratigraphic level) should be used to demonstrate the trace element variations within the Laacher See tephra (see Figs. 7, 8 and 9 in Wörner and Schmincke 1984), whereas additional petrographically distinct samples record the compositional range within a given layer (Table 1). In general, we observed compatible elements which show a continuous decrease in concentration from ULST to MLST with minimum values in the lowest LLST tephra (e.g. Sr, Sc, Co). Hybrid rocks are distinct in having very high contents

Table 2. Mineral and matrix trace element composition (ppm)

2.1 *Sanidine*

	1034 SAN	1060-5 SAN	1097-2 SAN	1017 SAN BR 2	1034 SAN BR 2	1060-5 SAN BR 2	1088-1 SAN BR 2	1097-2 SAN BR 2
Na %	3.71	2.77	2.99	5.06	4.26	3.10	2.9	2.83
K %	8.0	9.1	–	7.7	8.3	8.2	9.5	–
Ca %	–	–	–	0.17	0.25	0.31	0.36	–
Sc	0.03	0.031	–	0.0102	0.004	0.0071	0.0094	–
Cr	–	–	3.14	0.44	1.7	2.3	1.9	1.44
Fe %	0.13	0.17	0.17	0.113	0.138	0.168	0.164	0.156
Co	0.87[a]	0.90[a]	0.76[a]	0.046	–	0.058	0.034	0.067
Zn	4.36	–	–	1.32	–	–	–	–
Rb	128	124	111	175	134	133	126	110
Sr	434	1,381	1,712	114	490	1,500	1,766	1,687
Zr	–	–	–	7.2	–	–	–	–
Ba	1,189	3,296	3,920	64.3	1,238	3,651	4,057	3,497
La	7.61	10.4	11.5	4.5	10.8	12.8	13.2	10.4
Ce	4.57	5.47	7.10	1.9	4.4	6.33	6.65	6.0
Nd	–	3.38[b]	4.00[b]	–	–	–	–	0.59
Sm	0.032	–	0.04	0.009	0.016	0.028	0.031	0.036
Eu	0.37	0.75	0.92	0.15	0.41	0.86	0.96	0.96
Tb	–	–	–	–	–	–	–	–
Ho	–	–	–	–	0.044	0.11	0.11	–
Tm	–	–	–	–	–	–	–	–
Yb	–	–	–	0.007	–	–	–	–
Lu	–	–	–	–	–	–	–	–
Hf	0.25	–	0.63	0.26	–	–	–	–
Ta	–	–	–	–	0.04	0.05	–	0.04
Th	–	–	–	0.032	0.046	0.048	0.052	–
U	–	–	–	–	–	–	–	–

[a] Contamination during pelletizing procedure
[b] Interference of the 92.3 keV γ-line of ^{131}Ba on that of ^{147}Nd at 91.1 keV

2.2 *Plagioclase*

	1017 PLAG	1034 PLAG	1060-5 PLAG	1097-2 PLAG	1034 PLAG BR 2	1060-5 PLAG BR 2	1088-1 PLAG BR 2
Na %	6.05	4.58	4.53	4.21	4.8	5.4	4.78
K %	–	1.0	1.2	–	–	1.3	–
Ca %	–	–	–	–	2.4	4.2	2.6
Sc	0.35[a]	0.019	0.066	0.04	0.0083	0.0086	0.009
Cr	–	1.9[a]	–	–	2.1[a]	1.5[a]	–
Fe %	0.62	0.28	0.34	0.31	0.29	0.32	0.298
Co	7.14[b]	0.75[b]	0.90[b]	0.55[b]	0.014	–	–
Zn	–	–	9.11	–	0.14	2.7	3.6
Rb	–	–	–	–	4.1	6.7	3.0
Sr	3,577	3,218	3,430	3,180	2,987	3,638	3,510
Zr	–	–	–	–	–	–	–
Ba	1,167	933	1,150	951	931	1,126	1,033
La	32.5	29.1	27.3	26.2	32.9	33.6	31.6
Ce	8.59	23.0	24.2	24.9	21.9	30.4	25.9
Nd	–	3.39	4.32	3.21	3.8	6.3	2.26
Sm	0.48	0.18	0.26	0.30	0.27	0.36	0.32
Eu	1.44	0.99	1.22	1.17	0.98	1.22	1.16
Tb	–	–	–	–	0.014	0.02	0.02
Ho	–	–	–	–	–	–	–
Tm	–	–	–	–	0.0034	0.072[c]	–
Yb	–	–	–	–	0.0093	0.014	0.02
Lu	–	–	–	–	–	–	–
Hf	–	–	–	–	–	0.06	0.039
Ta	–	–	–	–	0.08	0.14	0.03
Th	–	–	–	–	0.044	0.12	–
U	–	–	–	–	–	–	–

[a] contaminated during mineral separation?
[b] contamination during pelletizing procedure
[c] unresolvable spectral interference of the 84.7 keV γ-line of ^{182}Ta on that of ^{170}Tm at 84.3 keV

Table 2 (continued)

2.3 *Hauyne*

	1034 HA	1088 HA	1060-5 HA	1034 HA BR 2	1060-5 HA BR 2	1088-1 HA BR 2
Na %	13.10	11.60	12.17	12.2	10.8	11.4
K %	–	–	–	–	–	–
Ca %	–	–	–	3.4	2.7	–
Sc	0.017	0.01	0.025	0.0150	0.0126	0.0072
Cr	1.93	–	–	0.5	–	–
Fe %	0.20	0.15	0.23	0.176	0.181	0.128
Co	0.36[a]	0.51[a]	0.33[a]	–	–	0.09
Zn	+	+	+	4.8	14.1	8.6
Rb	8.68	8.63	12.5	6.8	7.1	6.15
Sr	473	775	473	472	532	606
Zr	–	–	–	–	–	–
Ba	–	–	49.6	11.3	28.7	19.2
La	16.8	15.5	19.9	17.5	18.8	14.6
Ce	24.6	23.9	28.8	19.8	21.9	18.9
Nd	8.17	3.77	4.53	4.8	4.2	4.52
Sm	0.62	0.43	0.56	0.512	0.46	0.37
Eu	0.27	0.32	0.35	0.23	0.27	0.26
Tb	0.053	–	0.066	0.041	0.044	0.026
Ho	–	–	–	–	0.05	–
Tm	–	–	–	–	0.15	–
Yb	0.064	0.062	0.11	0.051	0.10	0.049
Lu	–	–	–	0.01	0.01	0.005
Hf	0.12	–	0.29	0.079	0.18	0.02
Ta	–	–	–	0.065	0.14	0.05
Th	0.34	0.13	0.78	0.34	0.50	0.071
U	–	–	–	–	0.13	–

[a] Contamination during pelletizing procedure

in compatible elements. The origin of these rocks is discussed elsewhere. Incompatible elements, in contrast, are enriched from ULST towards LLST. Most of the enrichment, however, takes place within the most differentiated LLST magma. Some other trace elements are depleted from ULST to MLST but show a reversed trend with concentrations increasing again from MLST towards LLST. These elements (e.g. Hf, Ta, Nd and Y; Wörner and Schmincke 1984) are referred to as "semicompatible" elements. Only two elements (Cr and Rb) behave indifferently which, in the case of Cr, is due to the low overall concentration and the (small) possibility of contamination of samples by Cr-bearing tools used during the preparation. Rb, on the other hand, could not be determined with sufficient accuracy using the INAA method. More reliable XRF data (Wörner and Schmincke 1984) show Rb to be a strongly enriched incompatible element with a regular trend. Rare earth elements (REE) show a non-uniform but systematic variation in concentrations and the chondrite-normalized patterns (Table 1 and Fig. 9 in Wörner and Schmincke 1984). Towards MLST and LLST, light and heavy REE are increasingly enriched with middle REE and especially Eu being strongly depleted relative to ULST magma.

These regular chemical variations are important evidence for the continuous eruption of the tephra from a single eruptive center successively tapping deeper layers of a single compositionally zoned magma chamber. Each sampled tephra layer represents a certain magma level within the reservoir prior to eruption. These compositional gradients may therefore be used for the chemical correlation of tephra layers (see Freundt 1982; Bogaard 1983). Compared to major element gradients of the Laacher See pyro-

2.4 *Amphibole*

						Magnetite		
	1017 AMPH	1060-5 AMPH	1034 AMPH	1088 AMPH	1099-2 AMPH	1017 MT	1060-5 MT	1088-1 MT
Na %	1.80	1.67	1.74	1.54	1.58	0.016	0.029	0.016
K %	1.0	2.0	2.3	2.2	2.1	–	–	–
Sc	14.6	17.5	18.1	16.7	15.2	0.70	2.10	1.68
Cr	7.21	7.84	–	12.1	–	6.77	13.0	12.1
Fe %	15.1	14.1	14.6	12.5	13.8	51.7	63.4	59.1
Co	20.7	28.5	30.3	24.9	23.4	24.5	61.6	61.5
Zn	124.6	139.5	145.4	128.8	161.8	774	669	607
Rb	–	–	–	–	–	–	–	–
Sr	342	750	565	919	–	–	–	–
Zr	340	562	–	166	207	–	–	–
Ba	274	706	709	513	535	–	–	–
La	109.2	79.5	86.6	74.2	78.0	11.4	33.6	26.9
Ce	215.3	224.8	231.7	335.2	216.1	14.7	63.2	51.0
Nd	87.4	118	112	126	102	6.04	23.9	21.6
Sm	10.8	17.4	15.1	17.3	16.9	0.45	2.82	2.42
Eu	2.91	5.18	4.04	3.81	4.74	–	0.65	0.58
Tb	1.31	1.85	1.77	1.76	2.03	–	0.62	–
Ho	–	2.28	–	0.93	2.29	–	0.54	–
Tm	0.49	0.94	0.50	0.75	0.57	–	–	0.14
Yb	3.94	4.68	4.66	4.45	4.75	–	0.70	0.90
Lu	0.85	0.66	0.69	0.62	0.82	–	0.12	0.11
Hf	12.7	7.94	8.73	6.69	7.87	0.75	0.94	0.83
Ta	4.36	6.58	5.97	6.66	6.01	0.84	5.07	3.13
Th	1.62	0.65	1.05	–	–	–	–	0.84
U	–	–	–	–	–	–	–	–

Table 2 (continued)

2.5 *Clinopyroxene*

	1034 CPX	1060-5 CPX	1088 CPX	1097-2 CPX[a]	1099-2 MEGA CPX	1099-2 CPX[a]	1017 CPX GREEN BR 2	1017 CPX GREY BR 2
Na %	0.61	0.86	0.71	0.40	0.32	0.35	0.82	0.59
K %	–	–	–	–	–	–	–	–
Ca %	–	–	–	–	–	–	9.1	10.6
Sc	22.7	23.7	25.8	102.1	111.4	107.9	24.8	43.4
Cr	12.9	5.3	12.5	413	819	432	6.5	61
Fe %	6.44	8.44	7.24	6.37	4.24	4.23	9.2	8.2
Co	17.6	15.5	15.3	209.7	30.7	29.4	18.5	26.8
Zn	–	110	–	–	–	–	–	–
Rb	–	–	–	–	–	–	5.2	–
Sr	–	–	–	–	–	–	–	–
Zr	–	315	–	–	–	–	511	352
Ba	–	–	–	–	–	–	–	–
La	33.2	45.2	36.1	8.04	4.7	5.6	70.0	22.9
Ce	92.4	138.2	118.1	24.5	18.5	21.3	149	75
Nd	67.6	85.3	60.6	18.4	19.5	15.6	69.7	69.4
Sm	11.3	13.5	13.4	4.75	3.83	4.22	12.0	13.9
Eu	3.52	3.87	3.63	1.33	1.22	1.25	3.65	4.3
Tb	1.10	1.64	1.69	0.64	0.64	0.52	1.5	1.8
Ho	1.65	1.64	1.98	0.48	–	0.60	1.6	2.0
Tm	–	0.31	0.19	0.39	–	–	0.42	0.26
Yb	2.81	5.29	4.75	1.02	1.50	0.92	4.0	3.20
Lu	0.37	0.64	0.53	0.09	0.12	0.19	0.46	0.35
Hf	8.11	11.2	9.43	4.05	3.44	3.84	11.6	10.7
Ta	1.32	1.67	1.33	0.29	–	–	2.54	2.04
Th	–	0.65	–	–	–	–	1.3	0.6
U	–	–	–	–	–	–	–	–

[a] Bulk clinopyroxene sample includes phenocrysts and cpx megacrysts

2.6 *Sphene*

	1017 SPH	1034 SPH	1044-1 SPH	1060-5 SPH	1075 SPH	1088-1 SPH	1089-1 SPH	1097-2 SPH
Na %	1.03	0.84	0.99	0.36	0.37	0.36	0.22	0.10
K %	–	–	–	–	–	–	–	–
Sc	1.06	0.91	0.87	1.33	1.50	1.60	1.93	1.36
Cr	24	29	27	25	34	–	–	69
Fe %	1.75	2.06	1.95	1.97	1.71	1.90	1.97	2.01
Co	4.5	1.6	3.5	2.1	1.7	3.5	2.8	5.8
Zn	–	–	–	–	–	–	–	–
Rb	–	–	–	–	–	–	–	–
Sr	–	–	–	–	–	–	–	–
Zr	2,788	2,667	1,536	1,817	1,073	2,139	2,854	1,913
Ba	401	599	728	904	1,390	1,285	1,482	1,605
La	2,306	2,840	2,358	2,619	2,507	2,603	2,653	2,698
Ce	6,060	7,400	6,513	7,752	7,405	7,760	8,098	8,226
Nd	2,098	2,557	2,546	3,358	3,291	3,520	3,790	3,856
Sm	241.4	306.8	309.7	443.9	444.9	477.2	512.5	510.3
Eu	46.6	59.4	64.0	94.0	97.0	103.7	114.3	113.7
Tb	25.3	32.7	31.8	47.8	47.9	51.2	54.4	52.5
Ho	64.7	40.2	62.9	52.6	50.5	53.5	64.2	96.4
Tm	8.64	17.4	9.07	22.6	23.3	25.6	24.8	22.5
Yb	60.3	73.6	69.9	88.3	85.6	92.3	95.4	99.0
Lu	8.82	10.10	9.94	15.4	14.3	16.1	16.3	14.0
Hf	114.4	134.7	102.6	103.6	96.7	100.8	103.2	101.2
Ta	441.1	544.7	486.0	555.9	576.3	602.4	610.4	665.9
Th	102.2	120.5	111.7	132.0	126.2	127.1	137.9	133.8
U	8.96	5.88	12.9	6.35	8.93	7.54	7.28	18.4

Table 2 (continued)

2.7 *Mica*

	1088-1 PHLOG	1089-2 PHLOG	1097-2 PHLOG	1088-1 PHLOG BR2	1089-2 PHLOG BR 2	1097-2 PHLOG BR 2	*Apatite* 1089-1 AP	*Olivine* 1097-2 OL
Na %	0.42	0.46	0.49	0.54	0.47	0.40	0.44	0.02
K %	6.53	6.33	6.69	–	–	–	–	–
Ca %	–	–	–	–	–	–	–	–
Sc	15.8	15.8	17.0	13.7	12.7	14.8	–	5.38
Cr	203	168	394	354	285	78.9	–	34
Fe %	9.99	10.15	9.17	7.9	7.64	6.44	0.53	16.87
Co	85.1	86.6	85.6	77.7	72.4	86.6	11.1	29.6
Zn	–	–	–	72	66	–	–	–
Rb	263	276	294	311	280	308	–	–
Sr	–	–	–	–	204	259	–	–
Zr	–	–	–	–	–	–	–	–
Ba	6,710	6,309	7,058	6,021	6,108	5,309	–	–
La	0.87	1.62	0.66	3.7	3.2	–	1,887	4.41
Ce	1.5	4.0	–	4.24	6.99	0.43	4,129	11.4
Nd	(9.2)[a]	(8.3)[a]	(7.4)[a]	1.96	3.62	–	1,710	5.3
Sm	0.09	0.17	0.04	0.23	0.50	0.029	197	0.71
Eu	–	0.12	0.07	0.128	0.30	0.061	45.9	0.18
Tb	–	–	–	0.04	0.05	–	20.7	0.09
Ho	–	–	–	–	–	–	13.0	0.22
Tm	–	–	–	0.09	0.07	0.05	–	–
Yb	–	0.09	–	0.1	0.129	–	27.4	0.25
Lu	0.08	–	–	0.049	0.054	0.020	2.36	0.03
Hf	1.52	0.85	0.96	0.35	0.51	0.29	–	0.26
Ta	1.23	1.31	1.12	2.05	2.33	0.80	–	0.79
Th	2.63	2.38	3.39	–	0.26	–	42.2	0.34
U	1.64	1.38	1.77	–	–	–	–	1.89
Ni	–	87.8	–	+	+	+	–	164.7

[a] See Table 2.1

2.8 *Matrix*

	1017 M	1034 M	1044-1 M	1050-1 M	1060-5 M	1088-1 M	1099-2 M
Na %	7.98	6.84	5.71	5.87	4.98	4.69	2.86
K %	6.8	8.7	–	–	6.2	8.9	7.0
Sc	0.13	0.15	0.38	0.35	0.45	0.59	16.8
Cr	–	4.68	7	5	2.53	–	133
Fe %	1.36	1.50	2.40	2.42	1.82	1.86	5.03
Co	0.57	0.65	1.1	1.0	1.62	1.84	25.5
Zn	102	75.7	60	62	43.6	39	–
Rb	320	231	177	186	130	134	88.5
Sr	21[a]	60[a]	156	167	258	301	534
Zr	928	688	627	739	318	340	450
Ba	178	127	194	209	595	599	1,384
La	161	131	103.8	107.9	97.9	100	78.7
Ce	204.5	170	152	160	143.7	162.8	153.2
Nd	34.6	31.5	29.0	29.8	37.5	41.1	31.9
Sm	2.25	2.07	3.02	3.06	2.87	4.00	7.97
Eu	0.31	0.45	0.63	0.68	1.10	1.17	2.02
Tb	0.39	0.50	0.36	0.38	0.19	0.25	0.87
Ho	–	–	–	–	–	–	–
Tm	0.53	0.44	0.28	0.24	0.47	0.54	0.37
Yb	4.46	3.11	2.44	2.52	2.01	2.12	2.31
Lu	0.78	0.64	0.43	0.48	0.31	0.35	0.29
Hf	23.5	15.0	10.5	10.7	7.29	7.50	6.62
Ta	5.13	4.79	5.14	5.10	5.63	6.30	5.07
Th	58.8	35.1	23.8	24.1	15.9	15.9	10.5
U	15.5	8.30	5.98	–	3.04	3.60	1.61

[a] XRF analysis from Wörner and Schmincke (1983)

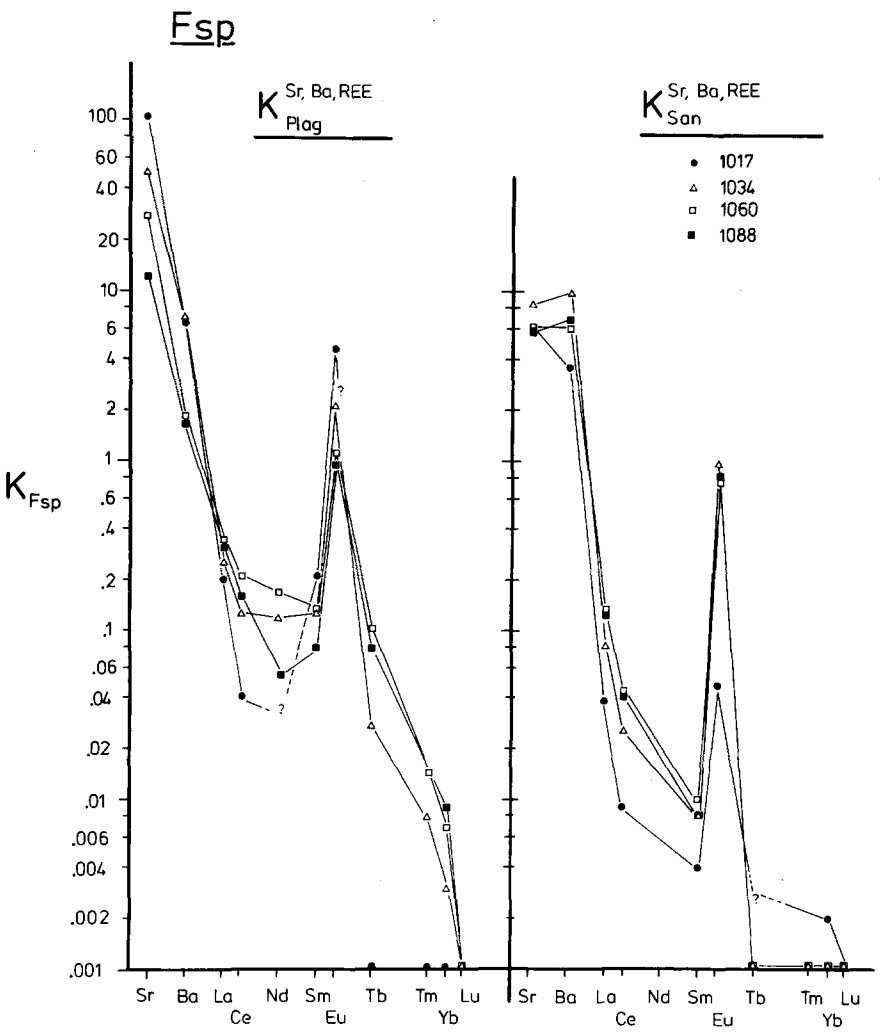

Fig. 2. REE and Sr and Ba distribution coefficient patterns ($K^{Sr,\ Ba,\ REE}$) for plagioclase and sanidine. Sample numbers refer to bulk samples of a particular sample layer, see Wörner 1982; Wörner and Schmincke 1984). 1017 = LLST, 1034 = MLST, 1060 and 1088 = ULST

clastic sequence (Wörner 1982; Wörner and Schmincke 1984), we find trace elements to be much more sensitive with regard to the compositional zonation and varying petrographic compositions (and thus the chemical homogeneity of a sampled layer).

Distribution coefficients

Ultra clean mineral and matrix separates were analyzed from four stratigraphic levels for trace elements by INAA (Table 2). Distribution coefficients (K) defined above are listed in Table 3. This coefficient K ideally represents the equilibrium constant for the exchange reaction:

$$TE_{(liquid)} + ME_{(solid)} = ME_{(liquid)} + TE_{(solid)}$$

(TE = trace element, ME = major element)

i.e. the equilibrium partition coefficient describing the partitioning of a trace element between growing phenocryst and host liquid. Disequilibrium between solid and liquid phase, kinetic and adsorption effects and a non-infinite melt reservoir as well as changing magma compositions due to "external" processes may cause the weight ratio C_s/C_l to deviate from the equilibrium partition coefficient. Here we report K values of 9 phenocryst phases including hauyne for a spectrum of whole rock and matrix major element and trace element compositions (Table 3). K-values for rare earth elements (K^{REE}) are plotted versus the atomic number resulting in easily comparable distribution coefficient patterns (e.g. Philpotts and Schnetzler 1970 and many others) in Figs. 2 to 6. A detailed comparison between Laacher See K-values of this study and literature data is given by Wörner (1982).

Feldspars. For sanidine, there is a good agreement between our K values and patterns (Fig. 2) and previously published K-feldspar distribution coefficients (e.g. Schnetzler and Philpotts 1970). Some plagioclase distribution coefficients, however, especially for Sr, Ba and Eu are larger by a factor of 2–3 when compared to literature data for intermediate calcalkaline rocks (Philpotts and Schnetzler 1970; Ewart and Taylor 1969; Nagasawa and Schnetzler 1970) and differentiated trachytic and alkaline rocks (Berlin and Henderson 1969 and Sun and Hanson 1976 respectively). Most remaining K values correspond to previously published data as do the K^{REE} patterns (Fig. 2) with the typical positive Eu-anomaly. As expected, Sr distribution coefficients are higher for plagioclase than for sanidine. On the other hand K^{Ba}_{San} and K^{Ba}_{Plag} are in same range (Table 3, Fig. 2). Some unusual conditions during feldspar crystallization must have allowed Ba to enter plagioclase as easily as sanidine. Significant Co and Sc concentrations were observed in some feldspars, which were irradiated in the reactor Thetis. These unusually high concentrations are most probably due either to impurities in the wax (or mineral separates), or were otherwise introduced during pelletizing. Indeed,

Table 3. Distribution coefficients (K)

3.1 *Sanidine*

	1034 SAN	1060 SAN	1097 SAN	1017 SAN BR 2	1034 SAN BR 2	1060-5 SAN BR 2	1088 SAN BR 2
Na	–	–	–	–	–	–	–
K	–	–	–	–	–	–	–
Sc	0.20	0.07	0.0	0.08	0.027	0.016	0.016
Cr	0.0	0.0	0.02	0.0	0.363?	0.909?	0.15?
Fe	–	–	–	0.0	0.092	0.092	0.088
Co	–	–	–	0.08	0.0	0.036	0.018
Zn	0.058	0.0	0.0	0.013	0.0	0.0	0.0
Rb	0.554	0.957	1.25	0.55	0.58	1.023	0.940
Sr	7.2	5.35	3.21	5.43	8.17	5.81	5.87
Zr	0.0	0.0	0.0	0.01	0.0	0.0	0.0
Ba	9.36	5.54	2.83	0.36	9.75	6.14	6.77
La	0.058	0.106	0.150	0.088	0.082	0.131	0.132
Ce	0.027	0.038	0.050	0.009	0.026	0.044	0.041
Nd	0.0	(0.090)	(0.130)	0.0	0.0	0.0	0.0
Sm	0.015	0.0	0.01	0.004	0.008	0.010	0.008
Eu	0.822	0.682	0.46	0.484	0.991	0.78	0.821
Tb	0.0	0.0	0.0	0.0	0.0	0.0	0.0
Ho	–	–	–	–	–	–	–
Tm	–	–	–	0.0	0.0	0.0	0.0
Yb	0.0	0.0	0.0	0.002	0.0	0.0	0.0
Lu	0.0	0.0	0.0	0.0	0.0	0.0	0.0
Hf	0.017	0.0	0.10	0.011	0.0	0.0	0.0
Ta	0.0	0.0	0.0	0.0	0.008	0.009	0.0
Th	0.0	0.0	0.0	0.001	0.001	0.0	0.003
U	0.0	0.0	0.0	0.0	0.0	0.0	0.0

3.2 *Plagioclase*

	1017 PLAG[a]	1034 PLAG[a]	1060 PLAG[a]	1097 PLAG[a]	1034 PLAG BR 2	1060 PLAG BR 2	1088 PLAG BR 2
Na	–	–	–	–	–	–	–
K	–	–	–	–	–	–	–
Sc	2.69	0.127	0.17	0.002	0.055	0.020	0.015
Cr	0.0	0.408	0.0	0.0	0.449	0.593	0.0
Fe	–	–	–	–	0.193	0.176	0.160
Co	–	–	–	0.021	0.022	0.0	0.0
Zn	0.0	0.0	0.21	0.0	0.002	0.062	0.092
Rb	0.0	0.0	0.0	0.0	0.018	0.052	0.022
Sr	170.3	53.6	13.3	5.96	49.8	14.10	11.66
Zr	0.0	0.0	0.0	0.0	0.0	0.0	0.0
Ba	6.56	7.35	1.93	0.69	7.33	1.892	1.725
La	0.200	0.222	0.279	0.330	0.251	0.343	0.316
Ce	0.042	0.135	0.168	0.160	0.129	0.212	0.159
Nd	0.0	0.108	0.115	0.100	0.121	0.168	0.055
Sm	0.213	0.087	0.091	0.040	0.130	0.125	0.080
Eu	4.65	2.2	1.11	0.58	2.178	1.109	0.991
Tb	0.0	0.0	0.0	0.0	0.028	0.105	0.060
Ho	–	–	–	–	–	–	–
Tm	–	–	–	–	0.008	–	0.0
Yb	0.0	0.0	0.0	0.0	0.003	0.007	0.009
Lu	0.0	0.0	0.0	0.0	0.0	0.0	0.0
Hf	0.0	0.0	0.0	0.0	0.0	0.008	0.005
Ta	0.0	0.0	0.0	0.0	0.017	0.025	0.0005
Th	0.0	0.0	0.0	0.0	0.001	0.008	0.0
U	0.0	0.0	0.0	0.0	0.0	0.0	0.0

[a] Very small amount of samples analyzed with large effects of possible contamination relative to blanks

3.3 *Hauyne*

	1034 HA	1060 HA	1088 HA	1034 HA BR 2	1060 HA BR 2	1088 HA BR 2
Na	–	–	–	–	–	–
K	–	–	–	–	–	–
Sc	0.11	0.06	0.08	0.10	0.028	0.012
Cr	0.41	0.0	0.0	0.107	0.0	0.0
Fe	–	–	–	0.117	0.099	0.069
Co	–	–	–	0.0	0.0	0.049
Zn	0.0	0.0	0.0	0.063	0.323	0.221
Rb	0.04	0.10	0.06	0.029	0.055	0.046
Sr	7.88	1.83	2.57	7.87	2.062	2.013
Zr	0.0	0.0	0.0	0.0	0.0	0.0
Ba	0.0	0.08	0.0	0.089	0.048	0.032
La	0.13	0.20	0.16	0.134	0.192	0.146
Ce	0.14	0.20	0.15	0.116	0.152	0.116
Nd	0.26	0.12	0.09	0.152	0.112	0.110
Sm	0.30	0.20	0.11	0.247	0.160	0.093
Eu	0.60	0.32	0.27	0.511	0.245	0.222
Tb	0.11	0.35	0.0	0.082	0.232	0.105
Ho	–	–	–	–	–	–
Tm	0.0	0.0	0.0	0.0	0.319	0.0
Yb	0.02	0.05	0.03	0.016	0.050	0.023
Lu	0.0	0.0	0.0	0.016	0.032	0.014
Hf	0.01	0.04	0.0	0.005	0.025	0.003
Ta	0.0	0.0	0.0	0.014	0.025	0.008
Th	0.01	0.05	0.01	0.010	0.031	0.004
U	0.0	0.0	0.0	0.0	0.043	0.0

samples irradiated in powder form in a sealed quartz ampoule (in the BR-2 reactor), have zero distribution coefficients for Sc and Co, as would be expected from the crystal chemistry of feldspars and literature data. Co and Sc in feldspars therefore most probably were introduced by contamination during and/or after the separation procedure.

Amphibole. There is a significant discrepancy between K_{Amph} values reported here and those known from the literature. For example, K_{Amph} for compatible elements (Ba, Sr, Sc) are larger by an order of magnitude compared to data by Philpotts and Schnetzler (1970), Ewart and Taylor (1969) and Nagasawa and Schnetzler (1970) for dacitic rocks and Sun and Hanson (1976) for a mafic phonolite. There are no reference values for $K_{Amph}^{Zn, Ta, Hf, Th, U}$. REE distribution coefficients (Table 3, Fig. 3) occupy the upper range of reported K_{Amph} data with similar K^{REE}-patterns (Fig. 3): The preference for the middle REE in amphiboles is more pronounced than previously reported by Schnetzler and Philpotts and others and is shown in strongly concave K^{REE} patterns for Laacher See amphiboles.

Clinopyroxene. Concentrations for K, Zn, Rb, Sr, Ba, Zr and U in clinopyroxene separates are below the limit of detection for all samples analyzed with INAA (except for a few containing Zn, Rb and Zr). The resulting zero K_{Cpx}-values correspond to the generally very low literature K_{Cpx}-values for these elements (e.g. Duncan and Taylor 1969; Phillpotts and Schnetzler 1970; Pearce and Norry 1970 for intermediate rocks and Larson 1979 for evolved alkaline host compositions). K_{Cpx}^{Sc} and K_{Cpx}^{REE} (Fig. 4) are 2–5 times larger than those reported by Sun and Hanson (1976) and Larson (1979). Clinopyroxene, like amphibole shows a

Table 3 (continued)

3.4 *Amphibole*

						Magnetite		
	1017 AMPH	1034 AMPH	1060-5 AMPH	1088 AMPH	1099-2 AMPH	1017 MT	1060-5 MT	1088 MT
Sc	112.3	120.7	38.89	28.3	0.90	5.38	4.67	2.85
Cr	0.0	0.0	3.10	0.0	0.0	0.0	5.14	0.0
Co	36.32	46.62	17.59	13.5	0.92	43.0	38.02	33.4
Zn	1.22	1.92	3.20	3.30	0.0	7.59	15.34	15.56
Rb	0.0	0.0	0.0	0.0	0.0	0.0	0.0	0.0
Sr	9.77	4	3	3.1	0.0	0.0	0.0	0.0
Zr	0.37	0.0	1.77	0.49	0.46	0.0	0.0	0.0
Ba	1.54	5.58	1.19	0.86	0.39	0.0	0.0	0.0
La	0.678	0.666	0.82	0.74	0.99	0.071	0.34	0.27
Ce	1.05	1.36	1.56	2.06	1.41	0.072	0.044	0.31
Nd	2.53	3.56	3.15	3.07	3.20	0.17	0.64	0.53
Sm	4.80	7.29	6.06	4.33	2.12	0.20	0.98	0.61
Eu	9.39	8.98	4.71	3.26	2.35	0.0	0.59	0.50
Tb	3.366	3.54	9.74	7.04	2.33	0.0	3.26	0.0
Ho	–	–	–	–	–	–	–	–
Tm	0.92	1.14	2.00	1.39	1.54	0.0	0.0	0.26
Yb	0.88	1.50	0.33	2.10	2.06	0.0	0.35	0.42
Lu	1.09	1.08	2.13	1.77	2.83	0.0	0.39	0.31
Hf	0.54	0.58	1.09	0.89	1.19	0.032	0.13	0.11
Ta	0.85	1.25	1.17	1.06	1.19	0.164	0.90	0.50
Th	0.028	0.030	0.041	0.0	0.0	0.805	0.0	0.053
U	0.0	0.0	0.0	0.0	0.0	0.725	0.0	0.0

3.5 *Clinopyroxene*

	1034 CPX	1060-5 CPX	1088 CPX	1099-2 MEGA-CPX	1099-2 CPX BULK	1017 CPX GREEN BR 2	1017 CPX BROWN BR 2
Na	–	–	–	–	–	0.103	0.074
Ca	–	–	–	–	–	–	–
Sc	151	52.7	43.7	6.62	6.41	191	334
Cr	2.76	2.09	0.0	6.16	3.25	3.25	30.50
Fe	–	–	–	–	–	6.76	6.03
Co	30.9	9.57	8.32	1.20	1.15	32.46	47.02
Zn	0.0	0.0	0.0	0.0	0.0	0.0	0.0
Rb	0.0	0.0	0.0	0.0	0.0	0.02	0.0
Sr	0.0	0.0	0.0	0.0	0.0	0.0	0.0
Zr	0.0	0.0	0.0	0.0	0.0	0.55	0.38
Ba	0.0	0.0	0.0	0.0	0.0	0.0	0.0
La	0.253	0.46	0.36	0.06	0.071	0.43	0.14
Ce	0.544	0.96	0.73	0.121	0.139	0.73	0.37
Nd	2.15	2.27	1.47	0.61	0.489	2.01	2.01
Sm	5.46	4.70	3.35	0.481	0.524	5.33	6.18
Eu	7.82	3.52	3.10	0.6	0.619	11.77	13.87
Tb	2.2	8.63	6.76	0.0	0.598	3.85	4.62
Ho	–	–	–	–	–	–	–
Tm	0.0	0.66	0.35	0.0	0.0	(0.79)	(0.49)
Yb	0.904	2.63	2.24	0.649	0.398	0.90	0.72
Lu	0.578	2.06	1.51	0.414	0.655	0.59	0.45
Hf	0.541	1.54	1.26	0.52	0.580	0.49	0.46
Ta	0.276	0.30	0.21	0.0	0.0	0.50	0.40
Th	0.0	0.04	0.0	0.0	0.0	0.022	0.01
U	0.0	0.0	0.0	0.0	0.0	0.0	0.0

strong preference for the middle REE (Fig. 4). Green Na-rich cpx and brown Ti-augite were separated and individually analyzed in only one sample (1017, LLST). Analytical results indicate significantly different trace element contents (and thus K-values) supporting the interpretation of a two-fold cpx population derived from the microprobe major element data (Wörner and Schmincke 1984). Green Na-augites have larger K's for incompatible elements (Zr, light and heavy REE, Hf, Ta, Th), brown Ti-augites, however, show larger distribution coefficients for Sc, Cr, Co and

Table 3 (continued)

3.6 *Sphene*

						Phlogopite		*Apatite*
	1017 SPH	1034 SPH	1044 SPH	1060 SPH	1088 SPH	1088 PHLOG	1088-1 PHLOG BR 2	1088 AP
Na	–	–	–	–	–	–	0.115	–
K	–	–	–	–	–	–	–	–
Sc	8.15	6.07	2.2	3.0	2.7	26.8	23.20	0.0
Cr	0.0	6.18	3.9	9.9	0.0	43.4	28.32	0.0
Fe	–	–	–	–	–	–	–	–
Co	7.89	2.46	3.2	1.3	1.9	46.3	42.23	6.03
Zn	0.0	0.0	0.0	0.0	0.0	0.0	1.846	0.0
Rb	0.0	0.0	0.0	0.0	0.0	1.1	2.321	0.0
Sr	0.0	0.0	0.0	0.0	0.0	0.0	0.0	0.0
Zr	3.0	3.88	2.5	5.7	6.3	0.0	0.0	0.0
Ba	2.25	4.72	3.8	1.5	2.1	11.2	10.1	0.0
La	14.3	21.7	22.7	26.8	26.0	0.007	0.037	14.4
Ce	29.6	43.5	42.8	53.9	47.7	0.009	0.026	24.3
Nd	60.6	81.2	87.8	98.5	85.5	–	0.048	54.3
Sm	107.3	148.2	102.6	154.7	119.3	0.043	0.058	95.2
Eu	150.3	132.0	101.6	85.5	88.6	0.0	0.109	102
Tb	64.9	65.4	88.3	251.6	204.8	0.0	0.160	41.4
Ho	–	–	–	–	–	–	–	–
Tm	16.3	39.5	32.4	48.1	47.4	0.0	0.167	0.0
Yb	13.5	23.7	28.7	43.9	43.5	0.0	0.047	8.81
Lu	11.31	15.8	23.1	49.7	46.0	0.13	0.140	3.69
Hf	4.87	9.0	9.8	14.2	13.4	0.10	0.047	0.0
Ta	86.0	113.3	94.6	98.7	95.6	0.26	0.325	0.0
Th	1.74	3.4	4.7	8.3	8.0	0.08	0.0	1.2
U	0.58	0.70	2.2	2.1	2.1	0.198	0.0	0.0

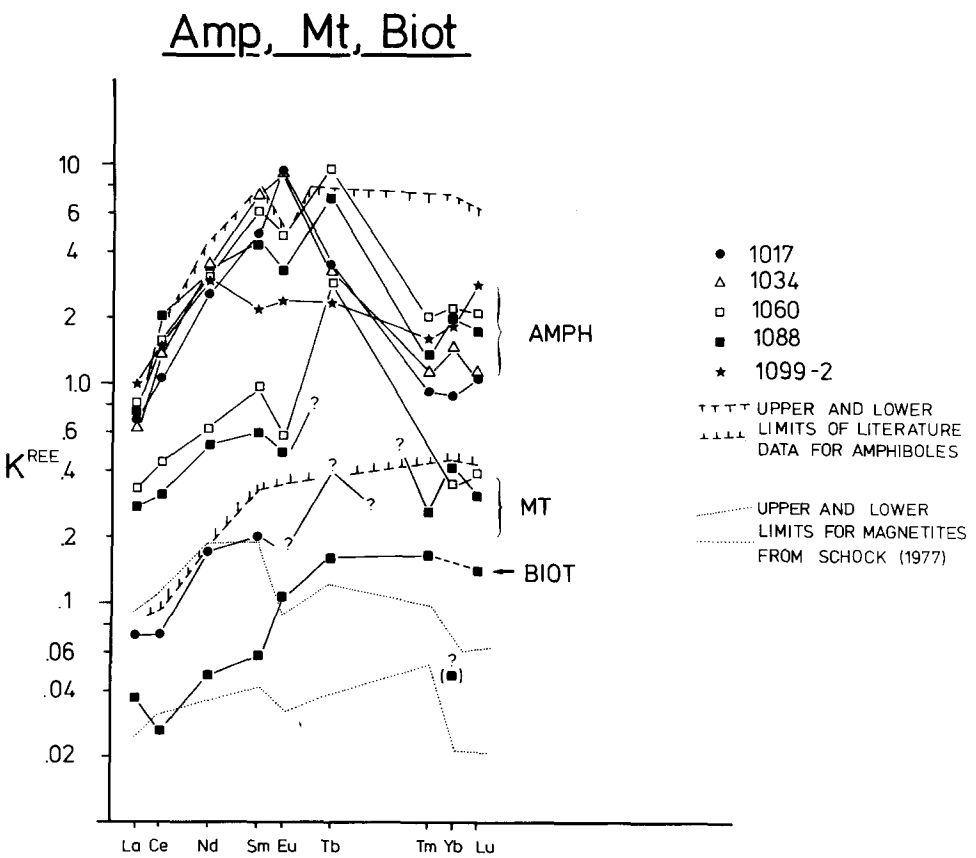

Fig. 3. REE distribution coefficient patterns for amphibole (Amp), magnetite (Mt) and mica (Biot = biotite/phlogopite). Sample numbers refer to bulk samples 1017 = LLST, 1034 = MLST, 1060 and 1088 = ULST, 1099-2 = mixed lava, upper ULST

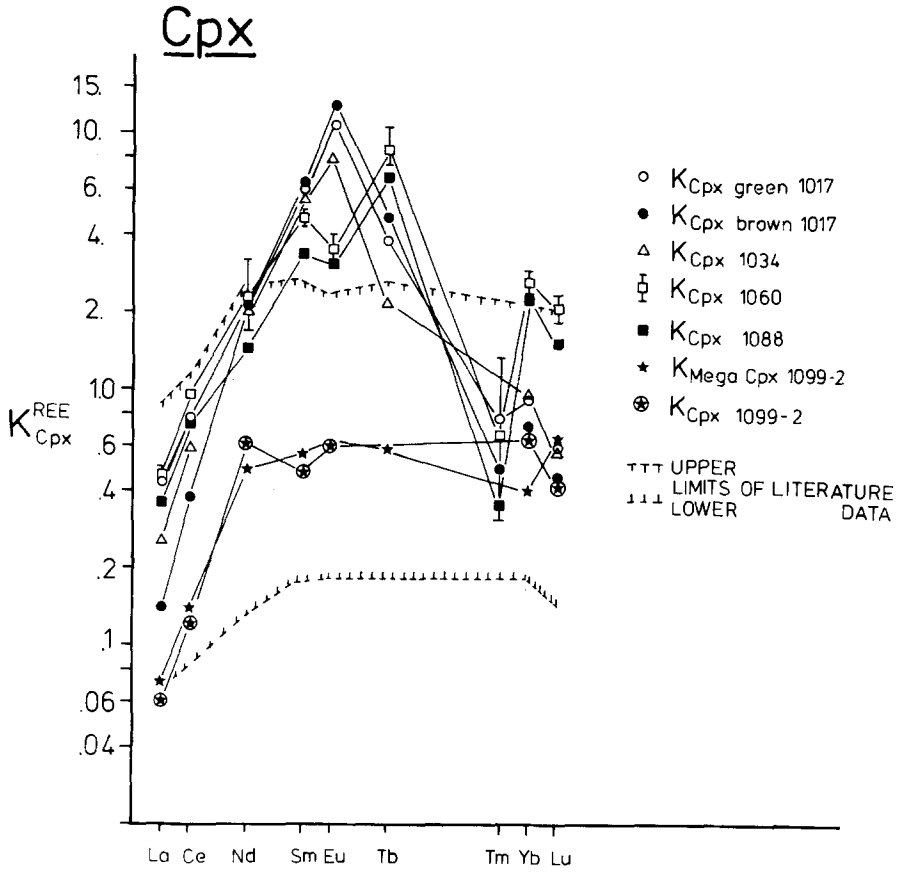

Fig. 4. REE distribution coefficient pattern for clinopyroxene (sample numbers see Fig. 6)

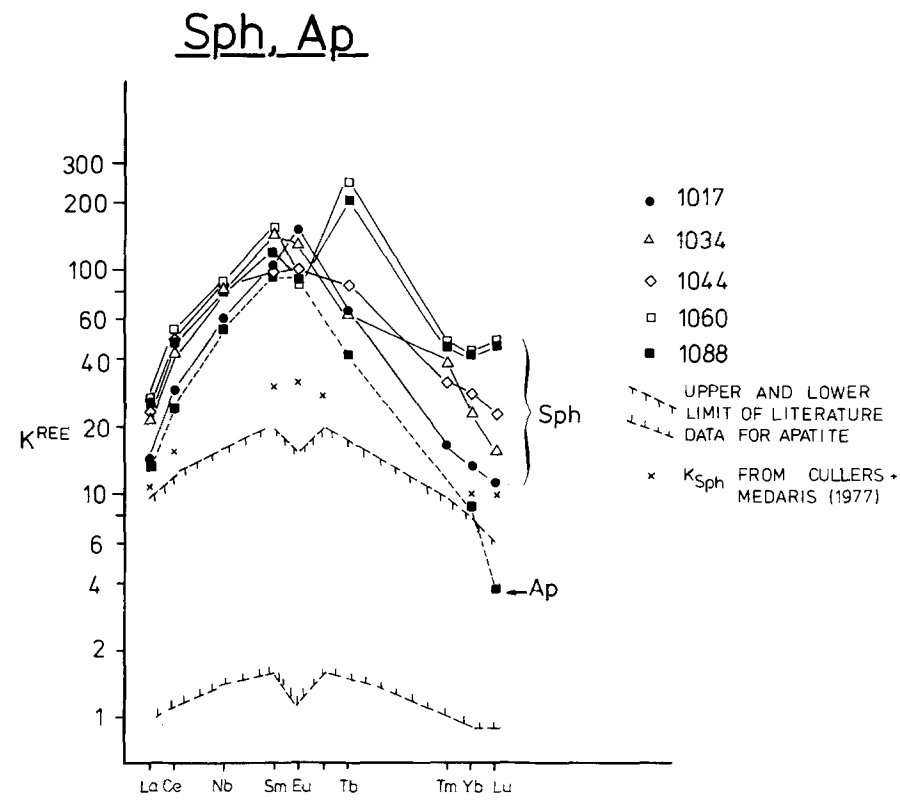

Fig. 5. REE distribution coefficient patterns for sphene (Sph) and apatite (Ap). Sample numbers see Fig. 6, 1044 = MLST

middle REE: compatible elements which are typical for the more "mafic" character of the Ti-augites.

Sphene. K^{REE}-values of Laacher See sphenes are significantly larger with a more pronounced concave K^{REE} pattern (Fig. 5) compared to data by Cullers and Medaris (1977). To our knowledge, there are no literature data for sphene/matrix pairs for Zr, Hf, Th, U, Ta (and Y, Nb for XRF data; Wörner 1982). However, large concentrations of these "incompatible" elements which result in large K_{sphene}

values (Table 3) are expected judging from the crystal chemistry of sphene which contain suitable sites for these elements (e.g. Ribbe 1980). Significant amounts of Sr, detected in Laacher See sphenes by XRF-analysis (Wörner 1982) could not be determined with INAA (Table 3, $K^{Sr}_{sphene}=0$) resulting in K^{Sr}_{sphene} being smaller than K^{Ba}_{sphene}, which is very unlikely in the light of the strong affinity between Ca and Sr. Judging from the XRF data of Wörner (1982), K^{Sr}_{sphene} may range from 15 to 20 which is more likely.

Magnetite, biotite and apatite. Magnetite REE distribution coefficients show an irregular pattern (Fig. 3) increasing from light to heavy REE. All values are significantly lower than those determined by Cullers and Medaris (1977) for alkaline rocks, but within the range reported by Schock (1977) for rhyodacitic to dacitic rocks, except for sample Mt 1017, which yields lower values. K^{Co}_{Mt} (Table 3), however, exceeds published values of Ewart et al. (1969) and Duncan and Taylor (1969) for host rocks of intermediate compositions by factors of 5 to 8 but is within the range reported by Schock (1977). K values for Sc agree well with the literature data. Our data for Cr are in the same order of magnitude as those of Ewart et al. (1969) and Duncan and Taylor (1969), but smaller than those of Schock (1977). Zn, Ta, Hf and Th distribution coefficients for magnetite determined here are similar to values of Schock (1977) except for sample Mt 1017 which exhibits lower K-values for Zn, and especially Ta and Hf; Th, on the contrary, is higher.

Biotite distribution coefficients for REE and incompatible elements are generally very low as would be expected from published values (Schnetzler and Philpotts 1970; Cullers and Medaris 1977). Only Sc, Cr, Co and Ba (+Rb) show $K>1$ (Table 3) (see also Schnetzler and Philpotts 1970; Andriambololona et al. 1975 and Arth 1976).

Apatite distribution coefficients for REE (Table 3), like those for sphene, are generally larger than the spectrum reported by Nagasawa (1970), Hart and Brooks (1974) and Sun and Hanson (1976). Again, there is a notable concave K^{REE} pattern (Fig. 5) emphasizing the preference of Laacher See phenocrysts for the middle REE. Except for Co (contamination??) and Th, all remaining K values are zero, data for a more detailed comparison are lacking.

Hauyne. To our knowledge, no trace element distribution coefficient data have been published for hauyne phenocrysts. Relative and absolute K values approach those of plagioclase (compare Figs. 2 and 6, Table 3), a probable result of substitution for Ca in both minerals. Therefore, distribution coefficients for Sr and Eu are highest (Fig. 6, Table 3) when compared to other trace elements in hauynes. Rb and Ba are only found in traces resulting in low K^{Rb}_{Ha} and K^{Ba}_{Ha}. The K^{REE} pattern (Fig. 6), which is similar to that of plagioclase, shows declining K^{REE} from light to heavy REE with a significant Eu anomaly. All other distribution coefficients (incompatible elements) are either zero or very small, again resembling plagioclase.

In summary, there is a general agreement between the magnitude and relative proportions of most distribution coefficients reported here and previously published values for intermediate to evolved and alkalic host magmas. Some values, however, are significantly larger or sometimes lower than those reported. These discrepancies were expected considering the large variation of distribution coefficients with

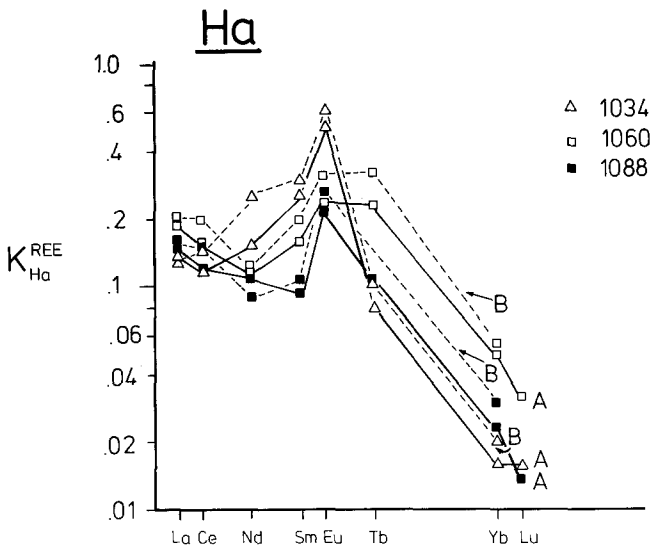

Fig. 6. REE distribution coefficient patterns for hauyne (Ha). Solid lines (A): analysed after irradiation with a neutron flux of 8×10^{13} n cm^{-2} s^{-1}. Dashed lines (B): analysed after irradiation with a neutron flux of 10^{12} n cm^{-2} s^{-1}. The agreement between the two data sets is fair, there is a slight shift towards lower REE distribution coefficients (contents) for hauynes analyzed after the BR-2 irradiation

host rock composition and the unusual major element composition of the Laacher See phonolite, for which comparison with literature data cannot be straightforward. Most Laacher See distribution coefficients for compatible elements are within or beyond the upper range of previously known values. On the other hand, those elements, for which low K values were reported in the literature, show zero distribution coefficients for the Laacher See phenocrysts. This result may only in part be due to concentrations being below the limit of detection of the INAA analytical method. We found that all minerals, which were known to incorporate middle REE in preference to heavy and/or light REE (Amph, Cpx, Sph, Ap) do so in a much more pronounced way for Laacher See phenocrysts (and possibly vice versa).

Discussion

Trace element abundances within the Laacher See phonolite sequence demonstrate the strong compositional zonation of the Laacher See magma column. The enrichment and depletion pattern is similar to the variation of trace elements in other compositionally zoned pyroclastic deposits (e.g. Hildreth 1979) and co-genetic series of moderately to strongly evolved volcanic rocks from a volcanic province (e.g. East Otago province, New Zealand; Price and Chappell 1975). In general, those elements which were shown to be incompatible to most Laacher See phenocryst phases (except sphene and apatite, which acted as traps for incompatible elements), are strongly enriched in the most differentiated LLST phonolite. Compatible trace elements, however, are extremely depleted within this upper part of the Laacher See magma column. The petrogenetic interpretation of the trace element variations is discussed elsewhere. Here we are mainly concerned with the discussion of trace element distribution coefficients and their variation within the rock suite studied. The variation of particular distribution coefficients was shown above to cover most of the range of published values from basaltic to rhyolitic host

rock compositions. For most elements, this variation shows a strong regular correspondence to the stratigraphic position of the samples analyzed. It is our aim to test all parameters which are known to govern the variation of distribution coefficients as possible causes for the variation of K which is observed for phenocrysts of the Laacher See phonolite sequence.

Temperature. A possible temperature gradient cannot account for the large variations of distribution coefficients observed: whenever a distribution coefficient was found to be temperature dependent, there *always* was an *increase* in K with *falling* temperature (Irving 1978; and others).

Pressure. Shimizu (1974) reported slightly pressure sensitive trace element distribution coefficients for clinopyroxene/melt pairs. Considering the small pressure gradient within the shallow level magma reservoir of the Laacher See magma system, it is not possible that the observed large variations in K are due to pressure effects.

f_{O_2}. The strong increase of the Eu distribution coefficients from ULST towards LLST could possibly be due to a *decreasing* oxygen fugacity (Drake 1975). However an effect on the other trace elements is very unlikely.

Mineral compositions. Recent studies by Watson (1977), Long (1978) and Hart and Davis (1978) have emphasized the influence of major element phenocryst composition on the mineral/matrix distribution of trace elements. However, only few phenocryst phases of the Laacher See phonolite in fact show variable major element compositions for different parts of the zoned magma column. However, *all* phenocrysts display the wide range of K values (except sanidine).

Growth rate and other kinetic effects. Albarede and Bottinga (1972), Dowty (1977), Long (1978) and Gamble and Taylor (1980) considered various kinetic effects during crystal growth as important parameters for trace element partitioning. However, phenocrysts within the Laacher See phonolite are similar in shape, zoning pattern and crystal size. This suggests that crystallization and thus trace element partitioning should have taken place under similar conditions. Therefore the above effects can be excluded.

Major element composition of the melt. The wide range of published distribution coefficient data for a particular type of phenocryst is generally attributed to variable melt compositions (basalt-rhyolite) and thus to a different degree of polymerization of the host silicate melt (Nagasawa and Wakita 1968; Nagasawa and Schnetzler 1971; Watson 1976, 1977; Reyerson and Hess 1978; Mysen and Virgo 1980; Mahood 1981 and Mahood and Hildreth 1983). Following the reasoning of Watson (1976), there should be a positive correlation between SiO_2 content (or degree of polymerization) of the melt and the partition coefficients. Wörner and Schmincke (1984) calculated the ratio of nonbridging oxygens to tetrahedra positions (NBO/T, see Mysen et al. 1981) as a measure of silicate network polymerization of the phonolitic Laacher See magma including the depolymerizing effect of volatile elements (H_2O, F, Cl). Resulting NBO/T values are low (more polymerized) for the lowest MLST units. Towards the most differentiated (alkali- and volatile-rich) LLST as well as towards the more mafic ULST compositions NBO/T increases from 0.18 towards 0.26 and 0.30 respectively, implying decreasing polymerization. If the variation of K were caused by variable host compositions (polymerization), we would expect maximum K values for *all* trace elements analyzed within the highly polymerized MLST phonolite magmas. However, the variation of K shows increasing values for incompatible elements only. Therefore, the gradients in major element composition (polymerization) cannot explain the variation of distribution coefficients observed.

Common parameters that might have affected the distribution coefficents within the Laacher See phonolite sequence were shown to be inadequate to explain the observed variations. Disequilibrium effects and trace element complexing are the only viable factors remaining. Trace element complexes, which may form in volatile rich magmas (Ringwood 1955a, b; Burns 1970; Bailey and MacDonald 1975) tend to stabilize these elements in the melt thus reducing its mineral/melt distribution coefficient. Watson (1979) found evidence for the existence of alkali-zircono-silicate complexes in silicate melts. Similar complexes which may or may not involve halogens and H_2O are probably formed by other trace elements with a high ionic potential (charge/radius, e.g. Ta, Hf, U, Th and REE, i.e. incompatible elements). We therefore have to consider trace element complexing within the volatile-rich upper (LLST) part of the Laacher See magma chamber as one possible cause for the observed decreasing K values towards LLST for some of these elements. Additional and/or alternative processes, however, have to be considered to explain distribution coefficients which are *increasing* towards LLST and other elements of distinct behavior. A comparison between trends of distribution coefficients and matrix compositions (Figs. 7–9) reveals that K values are highest for lowest trace element concentrations of the matrix (C_M) and vice versa. This negative correlation between K and C_M, which is found for all compatible and semicompatible trace elements as well (except Eu, Sr in sanidine), suggests some (matrix-) compositional control on the measured K values. Considering the failure of standard explanations, one possible way to produce such a correlation is to modify the trace element content of the matrix during or after the crystallization of phenocryst phases without re-equilibration between solid and liquid phase. If post-crystallization liquid-liquid differentiation processes were active within the upper parts of the Laacher See magma chamber we should expect the K values to be lowered (increased) by the same factor which is found to have increased (decreased) the trace element content of the magma after crystallization. This factor, of course, is not known. However, if we allow for a systematic error caused by the pre-existing trace element variations on which the effects of these late stage processes are superimposed it is possible to relate the variation of K expressed as $\Delta K = K_{LLST}/K_{ULST}$ to the variation of the matrix trace element composition ($\Delta M = C_{M,\,LLST}/C_{M,\,ULST}$) in a ΔK–ΔM-diagram (Figs. 10–12). Such a diagram summarizes the relationship between variable distribution coefficients and changing matrix composition, which is normalized for all elements by plotting the *relative* variation of K ($=\Delta K$) versus the *relative* variations in matrix composition $C_M (=\Delta M)$. Figures 10 and 11 display a quite close (inverse linear) relationship between the variation of K ($=\Delta K = K_{LLST}/K_{ULST}$) and matrix composition ($=\Delta M = C_{M,\,LLST}/C_{M,\,ULST}$) for most trace elements and phenocryst types (except for sani-

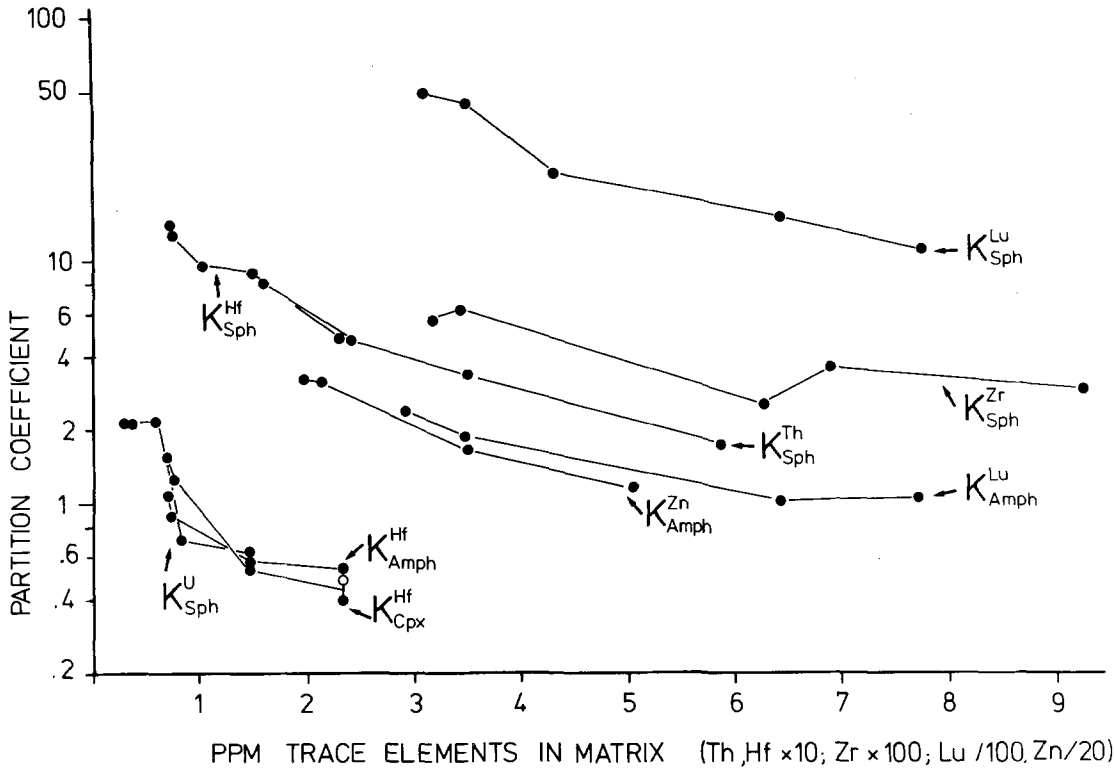

Fig. 7. Distribution coefficients for incompatible elements from different levels of the zoned phonolite sequence versus the trace element content of the corresponding matrix. Note the logarithmic scale for K

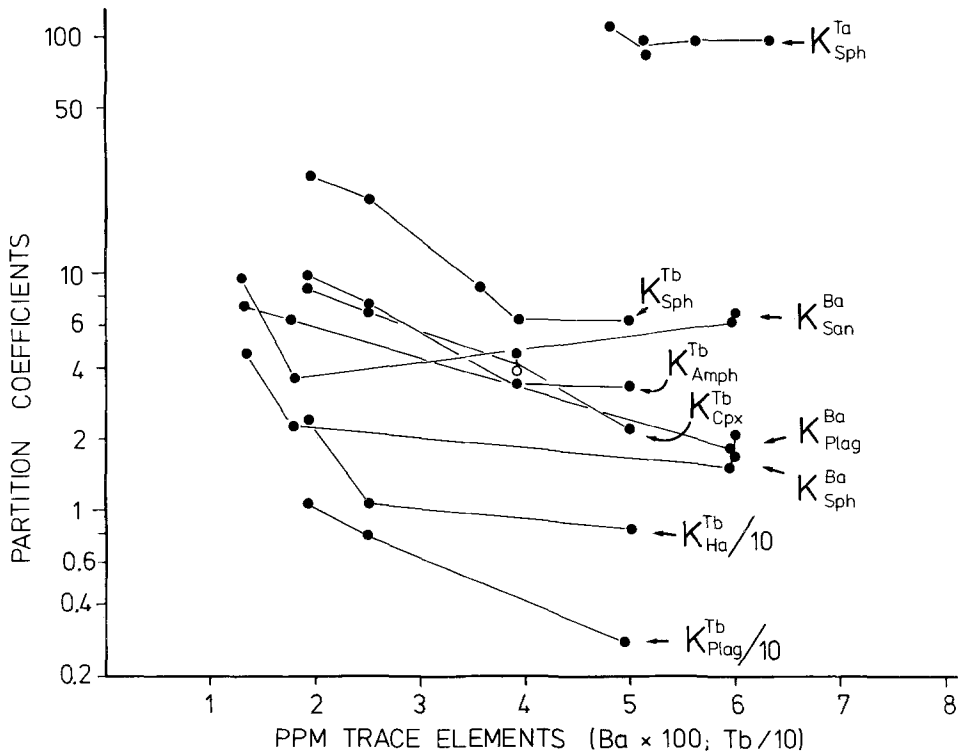

Fig. 8. Distribution coefficients for "semicompatible" elements (see Fig. 7). Note: Although there is a reversal of the matrix compositional trend (see text) there still is a good correlation to the variable distribution coefficients

dine, compatible elements). It is believed that such a diagram may be used to reveal the variation of K e.g. as a complex function of crystallization history and late stage (syn- to postcrystallization) differentiation processes. The crucial feature of this diagram is to interpret the position of particular data points relative to the different fields and lines portrayed in Fig. 12. A major constraint for the interpretation is the necessity (except for line VIII, Fig. 12) to exclude the possible influence on K by variable temperature, pressure and compositional parameters discussed above. For the Laacher See case, it was possible to reject these conventional explanations as a cause for the variation of K. However, other studies may find a close control of K by one or more of the above parameters. In such a case

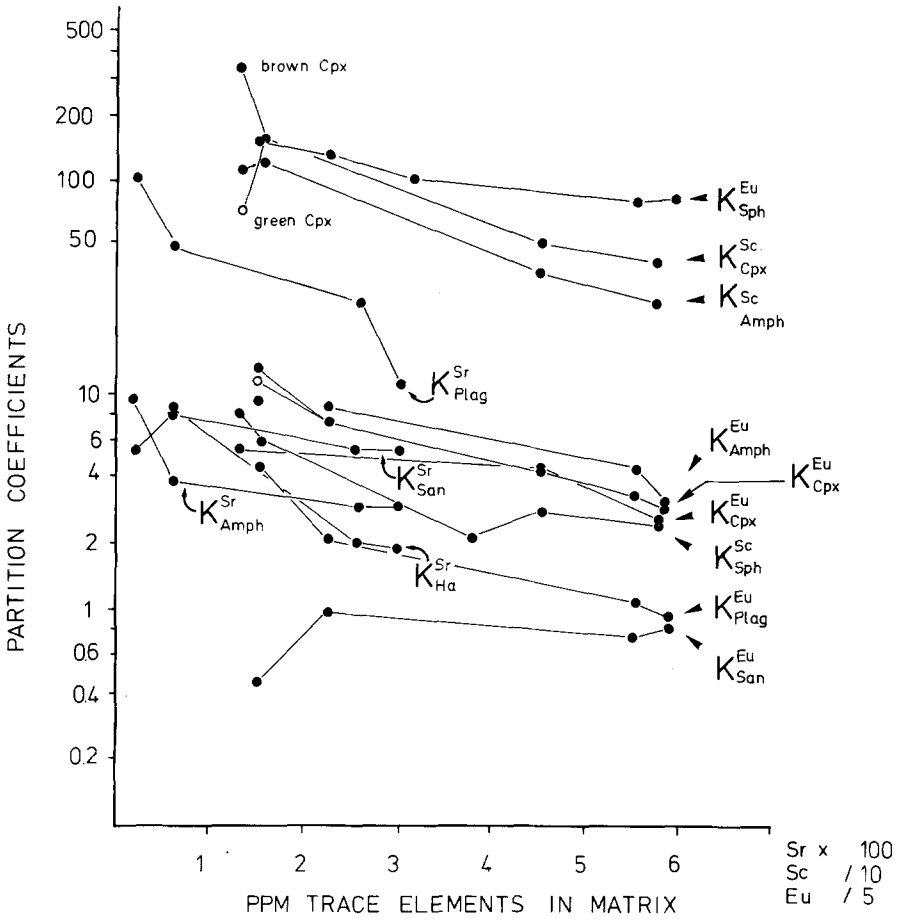

Fig. 9. Distribution coefficients for compatible elements versus matrix composition (see Figs. 7, 8)

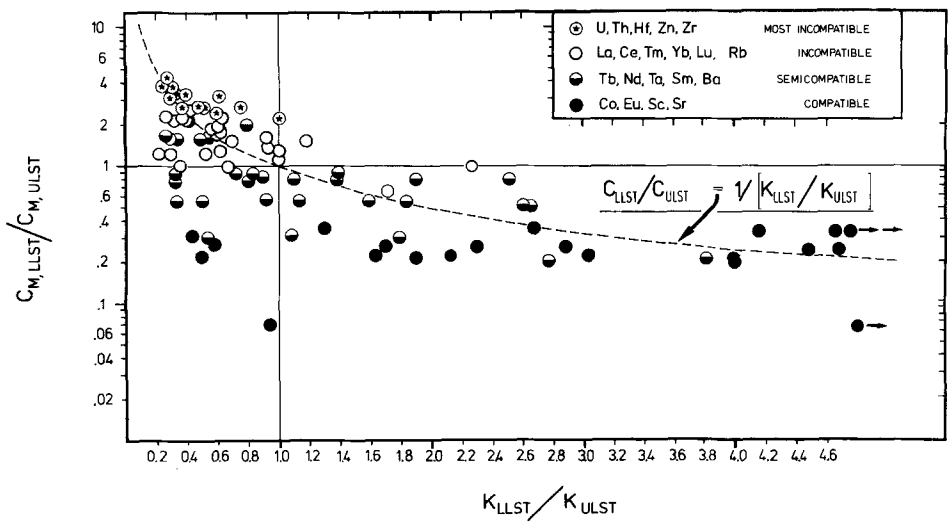

Fig. 10. Relative variation of K ($\Delta K = K_{LLST}/K_{ULST}$) versus the relative variation of matrix composition ($\Delta M = C_{M,\,LLST}/C_{M,\,ULST}$). Note the logarithmic scale for C_M; as a consequence, the inverse proportional relation between ΔK and ΔM ($\Delta K = 1/\Delta M$) is not a straight line but rather a ("exponential") curve. Data points are separated into four groups of trace elements (highly incompatible, incompatible, semicompatible and compatible)

we would expect, for constant matrix compositions, data points plotting near the horizontal line (I, VIII in Fig. 12) due to the variable K values ($\Delta M = 1$, $\Delta K > 0$). Only rising temperatures and reduced polymerization (which are unlikely conditions for a differentiating magma reservoir) and trace element complexing will reduce K ($\Delta K < 1$). For these instances, data points will fall to the left of the origin of the ΔK–ΔM-diagram on line I. Most of our ΔK–ΔM-pairs which plot in this region of the diagram in fact belong to those having a high ionic potential (the necessary condi-

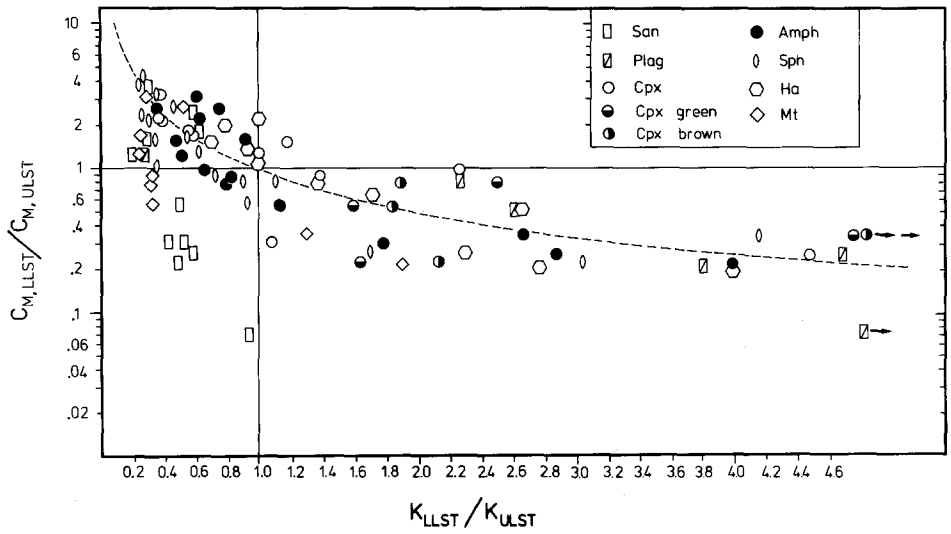

Fig. 11. ΔK–ΔM-diagram, for explanation see Fig. 10. Data points are distinguished for different phenocryst phases

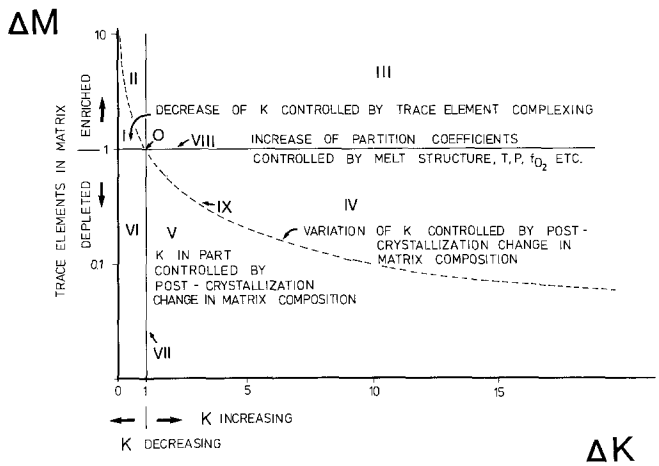

Fig. 12. The ΔK–ΔM-diagram. Different fields and lines (I–IX) are distinguished: The variation of K is explained on the basis of changing matrix (C_M) and phenocryst composition (C_s) following the definition of the distribution coefficient $K = C_S/C_M$. As a necessary condition, all additional parameters which could influence the equilibrium partition coefficient (such as P, T, f_{O_2} etc.) must be constant (except for line VIII, for which variable physical conditions and complexing at constant C_M are the only critical parameters. O = origin of the ΔK–ΔM-diagram, for which $\Delta K = \Delta M = 1$; K, C_M = constant

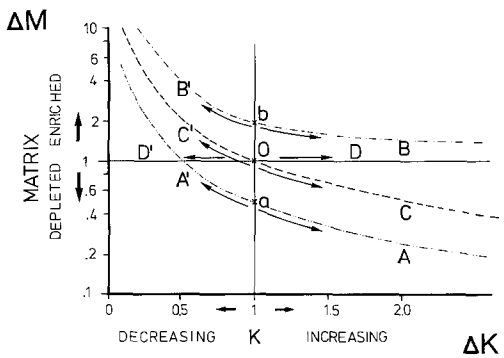

Fig. 13. Schematical ΔK–ΔM-diagram illustrating the 8 principal paths of changing K and C_M. Proceeding from O, these different evolutionary paths define the ΔK–ΔM-relationships during 50% open system crystallization with variable matrix composition, no re-equilibration between solid and liquid phase

tions to form complexes). Therefore it is likely that some of the distribution coefficients concerned were affected by complex building. On the other hand it is possible to have constant distribution coefficients for a wide range of matrix trace element compositions. This case applies to closed system equilibrium crystallization within a compositionally zoned magma chamber. As a consequence, we would find all data points plotting near the vertical line VII (Fig. 12) if temperature and pressure had only minor effects on K (which generally is the case). Most of our data points, however, which are plotted in the ΔK–ΔM-diagram fall near the dashed curve (IX) defined by the inverse proportional relation between the variation of K and the change in matrix composition (C_M). The position of data points relative to each other as well to the different lines discussed above is believed to bear some information on the evolution and relation to the ΔK and ΔM-pairs. Using Figs. 12 and 13 we will try to reconstruct possible evolutionary paths which may have lead to the observed position of data points in Figs. 10 and 11. We will try to interpret these different paths with regard to the complex crystallization history coupled with a postulated post- to syn-crystallization variation of matrix composition and other parameters:

– paths $O \rightarrow D$, $O \rightarrow D'$, $O \rightarrow b$ and $O \rightarrow a$.

These paths are equivalent to lines I, VII and VIII, which have been described above as defining variable physical and compositional parameters, complex building and equilibrium crystallization within a zoned magma column with variable matrix composition.

– path $O \rightarrow C$, $O \rightarrow C'$

follows the relation $1/\Delta M = \Delta K$ which designates the variation of K solely caused by post-crystallization modification of the matrix composition.

– path $O \rightarrow a \rightarrow A$ and A'

During equilibrium crystallization at $K > 1$ (with K = const., $\Delta K = 1$) the melt is depleted in compatible elements ($\Delta M = 0.5$ at a). At point a in Fig. 13, the particular phenocryst in question ceases to precipitate. Further crystallization of other phases may proceed and modify the trace element composition of the remaining melt. As a function of their overall K_{bulk}, the trace element content of the matrix will

be reduced or raised (path $a \rightarrow A$ or $a \rightarrow A'$). As an alternative explanation for the variation of the matrix composition we envisage liquid controlled differentiation processes that became active after the formation of phenocrysts or by settling or crystals in deeper magma layers of different composition. If one now separates and analyses such a mineral – matrix pair, the measured K values will be reduced (raised) relative to the original equilibrium distribution coefficient. Following this reasoning, we would anticipate compatible element ΔK–ΔM pairs to follow path $O \rightarrow a \rightarrow A$ and consequently to plot in field V of Fig. 12, which is the case. Semicompatible elements, which per definition are depleted first and then enriched during the course of the magmatic evolution (e.g. Ta) should follow path $O \rightarrow a \rightarrow A'$ and thus fall in field VI of Fig. 12, which, in fact most semicompatible elements do.

– path $o \rightarrow b \rightarrow B$ and B'

50% equilibrium crystallization of phenocrysts with $K \ll 1$ under constant conditions will result in the enrichment of all incompatible elements by a factor of 2. Distribution coefficients, however, remain constant ($\Delta K = 0$, $\Delta M = 2$, $o \rightarrow b$). Further enrichment due to the crystallization of the remaining phases or modification of the trace element content of the matrix by one of the above processes will cause the K-value of a certain phenocryst to increase or decrease after the end of its crystallization ($b \rightarrow B$, $b \rightarrow B'$). Except for crystals settling into less evolved magma layers, there is no plausible mechanism to *reduce* the concentration of an incompatible element within the matrix during the evolution of the magma body. Therefore, *no* ΔK–ΔM pairs are expected to follow path $o \rightarrow b \rightarrow B$ and thus to fall in field III of Fig. 12. Figures 10 and 11 only show one data point (K_{cpx}^{La}) plotting in field III. Therefore we conclude that settling of the phenocrysts analyzed cannot have played a role in the variation of K for the incompatible elements concerned. On the other, hand we find most of the ΔK–ΔM pairs for incompatible elements just within field II which corresponds to path $o \rightarrow b \rightarrow B'$ described above. This is in agreement with post-crystallization enrichment of these incompatible elements in the host matrix. As late stage differentiation processes may become operative at any point late in the evolution of the crystallizing magma chamber, we expect that any point in the ΔK–ΔM-diagram may be displaced from any original position on lines parallel to but displaced from line IX (e.g. $a \rightarrow A$, $b \rightarrow B'$) which defines the inverse relation between ΔM and ΔK. In addition, trace element complexing and variable $P/T/X$ conditions, the latter of which were shown to have only minor effects on the K values within the Laacher See magma chamber, theoretically could also become operative during magmatic evolution. Such effects would result in a shift of data points parallel to the ΔK-axis (variable K at constant C_M).

As was shown earlier, there are no conventional explanations for the observed large variations of distribution coefficients within the Laacher See magma chamber. However, a number of geologically reasonable explanations are obtained from the interpretation of data points within the ΔK–ΔM-diagram. Moreover, the agreement between the geochemical character of a certain trace element and the position of its ΔK–ΔM-pairs with regard to the different fields and lines of the ΔK–ΔM-diagram suggests that the evolutionary paths developed for the different areas may correctly describe the evolution of the mineral/matrix pairs. Thus, we propose that large variations of distribution coefficients for mineral phases within the Laacher See phonolitic magma column were caused by a variation of the matrix composition *after* the precipitation of the phenocrysts. This model calls for some process which could have modified the trace element composition of the phonolite at a late stage of its differentiation and crystallization history: In summary, there are three possible mechanisms, some of which have already been mentioned:

a) After the crystallization of a particular phenocryst phase, the composition of the matrix is further modified by ongoing crystallization of other phases with no re-equilibration of early crystallizing phases.

b) Enrichment or depletion of certain trace elements due to late stage, liquid controlled differentiation processes.

c) Mixing of two melts of different trace element composition will also modify the mineral – melt distribution coefficients as will crystal settling into lower magma layers.

In any case, there cannot have been significant re-equilibration between minerals and the modified melt due to slow diffusion in the solid phase. Some re-equilibration which could have occurred at the extreme rims of the phenocrysts can probably only be detected by ion probe scans. On the other hand, trace element analyses of glass inclusions and comparison with the matrix composition adjacent to the crystal concerned, would further help to put constraints upon the type and characteristics of the process involved.

Hildreth (1979) reported major and trace element data on whole rocks and phenocrysts from the rhyolitic Bishop Tuff ignimbrite which was erupted from the top of the Long Valley magma chamber. In the ΔK–ΔM diagram the Bishop Tuff distribution coefficients are plotted versus the variation of whole rock composition (Fig. 14) which seems to be permissible for these generally phenocryst-poor rocks. Data points for the Bishop Tuff scatter around the vertical line (VII in Fig. 12) indicating large variations in melt compositions at rather uniform K-values (Fig. 14). Following the reasoning developed above, this result should indicate equilibrium crystallization within a compositionally zoned magma chamber and K being largely independent of P, T and X. There is no clear evidence for post-crystallization processes affecting the mineral – melt trace element ratios. These findings are in close agreement with those of Hildreth (1979), who proposed equilibrium crystallization without crystal settling subsequent to and independent from the development of the compositional variation within the zoned Long Valley magma chamber. However, Mahood and Hildreth (1983) concluded that "some rhyolitic partition coefficients depend in part on the concentration of the trace element itself". This could indicate – at least for some elements and to a much smaller extent – that processes similar to the ones postulated here influenced the measured trace element distribution between phenocrysts and Bishop Tuff magma.

Mahood (1981) and Mahood and Hildreth (1983) also reported distribution coefficients for a series of rocks erupted from the Sierra La Primavera complex (Mexico). The wide range of distribution coefficients was attributed to the slightly variable major and largely different volatile compositions of the host rhyolites which in turn resulted in different degrees of polymerization of the silicate melt. In accordance with the model developed here, the data of Mahood (1981) plot on or near the horizontal line (VIII, Figs. 12, 14), which defines a variation of K being caused

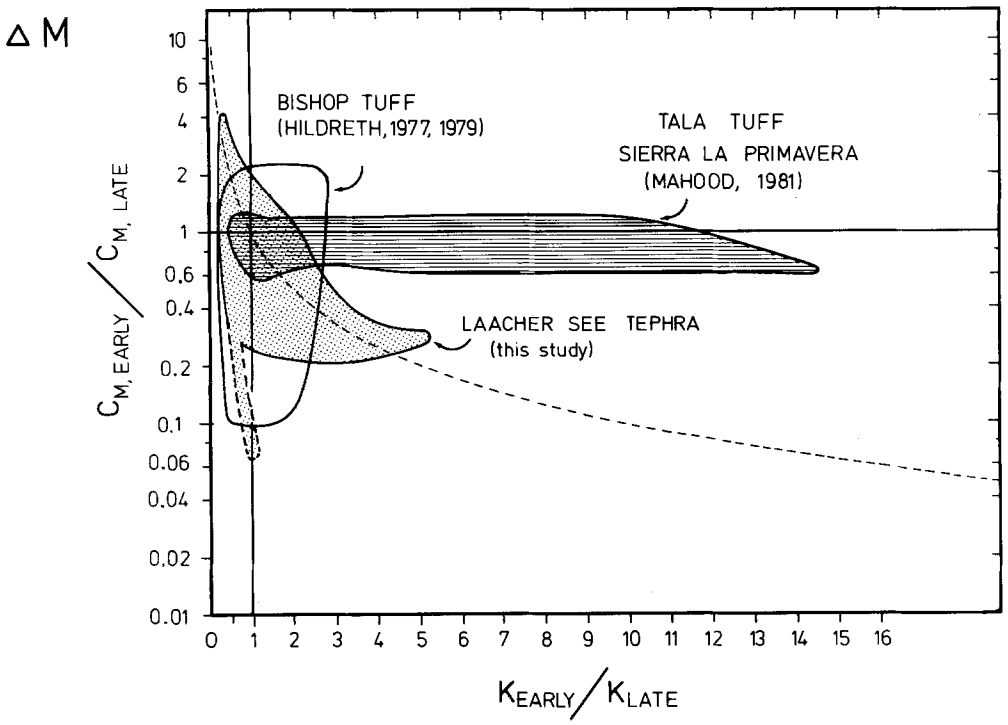

Fig. 14. ΔK–ΔM-diagram with data from the rhyolitic Bishop Tuff (California; Hildreth, 1979) and rocks from the Sierra La Primavera (Mexico; Mahood, 1981) and the Laacher See phonolite sequence. There are three fields of ΔK–ΔM-pairs distinguished which are explained in the text

either by variable temperature, pressure, f_{O_2} *or polymerization* of the melt. This agreement between the interpretation based on our model and independent but equivalent interpretations by Hildreth (1979), Mahood (1981) and Mahood and Hildreth (1983) strongly supports our model developed for the phenocryst/matrix pairs of the Laacher See phonolite suite. More detailed geochemical investigations on zoned magmatic systems are clearly needed to test this interpretation and the use of ΔK–ΔM-diagrams.

Conclusions

The present study reports trace element abundances within a series of whole rock samples and mineral/matrix pairs from the late Quaternary phonolitic Laacher See pyroclastic sequence. Bulk and matrix samples display a striking trace element variation within the section analyzed, which is interpreted as the result of an eruption from a compositionally zoned magma column.

Incompatible elements show a systematic enrichment towards the roof of the magma chamber. Compatible elements form gradients with lowest concentrations at the top and largest contents within lowest parts of the erupted magma column. Semicompatible elements show a strong depletion towards more differentiated magma compositions. However, towards the most differentiated top of the reservoir these elements display a strong enrichment leading to an inversion of the gradient at intermediate sample levels. Only few trace elements, which are typically depleted within the Laacher See phonolite sequence, show no systematic variation. These trace element gradients serve to better define and characterize the compositional zonation within the Laacher See magma chamber prior to eruption. Measured trace element abundances and the observed enrichment and depletion patterns place important constraints on petrogenetic models for the evolution of the zoned Laacher See magma chamber.

Mineral/melt trace element distribution coefficients were obtained from analyzing a large number of mineral and matrix separates. These K-values were shown to belong to the upper range of previously determined distribution coefficients for the phenocrysts concerned. Differential incorporation of trace elements into the crystallizing solid phase seems to be more pronounced for mineral/matrix pairs from the Laacher See phonolite: elements, which were shown by previous distribution coefficient studies to be compatible with regard to a certain mineral phase, are even more so for phenocrysts from the Laacher See phonolite. On the other hand, most elements known to be incompatible (very low K) could not even be detected by INAA of the mineral separates. The most striking characteristic of the observed mineral/matrix distribution coefficients is their extreme variation within the phonolite sequence, which displays a close (inverse) correlation to the trace element contents of the corresponding matrix. A detailed investigation of this relationship using the ΔK–ΔM-diagram shows the probable influence of late stage differentiation processes which modified the trace element composition of the melt mainly subsequent to phenocryst precipitation. As a result, measured mineral/melt concentration ratios do not reflect equilibrium partition coefficients because re-equilibration between the solid and liquid phase did not occur. The large variations of K therefore depend on the sensitivity of a certain trace element to, and the extent of, post-crystallization liquid-liquid differentiation processes. The exact nature, however, of these processes cannot be resolved by means of the ΔK–ΔM-diagram. A comparison between the Laacher See zoned magma chamber and other, rhyolitic zoned systems demonstrates the validity of the ΔK–ΔM-diagram and its interpretation developed here. Trace element modelling in highly evolved magma systems based on distribution coefficient data obtained by analyses of the rocks, matrix and phenocrysts concerned, have to take into account the possibility of late stage differentiation processes which may affect the trace element composition of the melt (matrix) subsequent to the precipitation of the phenocrysts

and thus may severely modify the measured mineral/melt trace element distribution.

Acknowledgements. Major parts of the present study are based on a joint project which was funded by the European Commission, contract numbers 230-77-EGD (grant to H.U.S.) and 219-77-EGB (grant to R.G.). Further financial support was granted to H.U.S. by the Bundesministerium für Forschung und Technologie, Bonn (BMFT, grant no. ET 4122 A) and the Ministerium für Forschung und Wissenschaft Nordrhein Westfalen (MWF, grant no. MWF-FA-9269 and FA-9444). During the early stages of the work, G.W. was supported by the Studienstiftung des Deutschen Volkes.

References

Albarede F, Bottinga Y (1972) Kinetic disequilibrium in trace element partitioning between phenocrysts and host lava. Geochim Cosmochim Acta 36:141–156

Andriambololona R, Lefèvre C, Dupuy C (1975) Coefficient de partage des éléments de transition dans les minéraux ferro-magnésiens extraits des dacites. C.R. Acad Sci Paris, série D, 287

Arth JG (1976) Behavior of trace elements during magmatic processes – a summary of theoretical models and their applications. J Res US Geol Surv 4:124–150

Bailey DK, MacDonald R (1975) Fluorine and chlorine in peralkaline liquids and the need for magma generation in an open system. Mineral Mag 40:405–414

Barberi F, Bizouard H, Clochiatti R, Metrich N, Santacroce R, Sbrana A (1981) The Somma-Vesuvius magma chamber: A petrological and volcanological approach. Bull Volcanol 44:295–316

Berlin R, Henderson CMB (1969) The distribution of Sr and Ba between alkalifeldspar, plagioclase and groundmass phases of porphyritic trachytes and phonolites. Geochim Cosmochim Acta 33:247–255

Bogaard vdP (1983) Die Eruption des Laacher See Vulkans. Ruhr Universität Bochum, PhD Thesis, pp 1–348

Burns RG (1970) Mineralogical applications of crystal field theory. Cambridge University Press, pp 1–223.

Cullers RL, Medaris G Jr (1977) Rare earth elements in carbonatites and cogenetic alkaline rocks: Examples from Seabrook Lake and Callander Bay, Ontario. Contrib Mineral Petrol 65:143–153

Dowty E (1977) The influence of adsorption in igneous partitioning of trace elements. Geochim Cosmochim Acta 41:1643–1646

Drake MJ (1975) The oxidation state of europium as an indicator of oxygen fugacity. Geochim Cosmochim Acta 39:55–64

Duda A, Schmincke HU (1978) Quaternary basanites, melilite nephelinites and tephrites from the Laacher See Area, Germany. N Jb Mineral Abh 132:1–33

Duncan AR, Tylor SR (1969) Trace element analysis of magnetites from andesitic and dacitic lavas from Bay of Plenty, New Zealand. Contrib Mineral Petrol 20:30–33

Ewart A, Taylor JR, Capp A (1968) Geochemistry of the pantelleriites of Mayor Island, New Zealand. Contrib Mineral Petrol 17:116–140

Ewart A, Taylor SR (1969) Trace element geochemistry of the rhyolitic rocks, central North Island, New Zealand, phenocryst data. Contrib Mineral Petrol 22:127–146

Freundt A (1982) Stratigraphie des Brohltal-Trass und seine Entstehung aus pyroklastischen Strömen des Laacher See Vulkans. Diplomarbeit (M.A. Thesis), Ruhr-Universität Bochum, unpubl., pp 1–320

Gamble RP, Taylor LA (1980) Crystal/liquid partitioning in augite: Effects of cooling rate. Earth Planet Sci Lett 47:21–33

Gibson IL (1970) A pantelleritic welded ash-flow tuff from the Ethopian rift system. Contrib Mineral Petrol 28:89–111

Häkli TA, Wright TL (1967) The fractionation of nickel between olivine and augite as a geothermometer. Geochim Cosmochim Acta 31:877–884

Hanson GN (1978) The application of trace elements to the petrogenesis of igneous rocks of granitic composition. Earth Planet Sci Lett 38:26–43

Hart SR, Brooks C (1974) Clinopyroxene-matrix partitioning of K, Rb, Cs, Sr and Ba. Geochim Cosmochim Acta 38:1799–1806

Hart SR, Davis K (1978) Nickel partitioning between olivine and silicate melts. Earth Planet Sci Lett 40:203–219

Hertogen J (1974) Instrumentele Neutronenactiveringsanalyse van Silikaatgesteenten. PhD Thesis, University of Ghent (Belgium), pp 1–230

Hertogen J, Gijbels R (1971) Instrumental neutron activation analysis of silicate rocks with a low-energy photon detector. Anal Chim Acta 56:61–82

Hildreth W (1977) The magma chamber of the Bishop Tuff: Gradients in temperature, pressure, and composition. PhD Thesis, Berkeley, Univ of California, pp 1–328

Hildreth W (1979) The Bishop Tuff: Evidence for the origin of compositional zonation in silicic magma chambers. In: Chapin CE, Elston WE (eds) Ash-Flow Tuffs, Geol Soc Am Spec Pap 180: pp 43–75

Hildreth W (1981) Gradients in silicic magma chambers: Implications for lithosphere magmatism. J Geophys Res 86 B11:10153–10192

Irving AJ (1978) A review of experimental studies of crystal/liquid trace element partitioning. Geochim Cosmochim Acta 42:743–770

Jacobs JW, Korotev RL, Blanchard DP, Haskin LA (1977) A well tested procedure for instrumental neutron activation analysis of silicate rocks and minerals. J Radioanal Chem 40:93–114

Larsen LM (1979) Distribution of REE and other trace elements between phenocrysts and peralkaline undersaturated magmas, exemplified by rocks from the Gardar igneous province, South Greenland. Lithos 12:303–315

Long PE (1978) Experimental determination of partition coefficients for Rb, Sr and Ba between alkali feldspar and silicate liquid. Geochim Cosmochim Acta 42:833–846

Mahood G (1981) Chemical evolution of a Pleistocene rhyolitic center: Sierra La Primavera, Jalisco, Mexico. Contrib Mineral Petrol 77:129–149

Mahood G, Hildreth W (1983) Large partition coefficients for trace elements in high silica rhyolites. Geochim Cosmochim Acta 47:11–30

Mysen BO, Virgo D (1980) Trace element partitioning and melt structure: An experimental study at 1 atm. Geochim Cosmochim Acta 44:1917–1930

Mysen BO, Virgo D, Kushiro I (1981) The structural role of aluminium in silicate melts – a Raman spectroscopic study at 1 atmosphere. Am Mineral 66:678–701

Nagasawa H (1970) Rare earth concentrations in zircons and apatites and their host dacites and granites. Earth Planet Sci Lett 9:359–364

Nagasawa H, Wakita H (1968) Partitioning of uranium and thorium between augite and host lavas. Geochim Cosmochim Acta 32:917–921

Nagasawa H, Schnetzler CC (1971) Partitioning of rare earth, alkali and alkaline earth elements between phenocrysts and acidic igneous magma. Geochim Cosmochim Acta 35:953–968

Pearce JA, Norry MJ (1979) Petrogenetic implications of Ti, Zr, Y and Nb variations in volcanic rocks. Contrib Mineral Petrol 69:33–47

Philpotts JA, Schnetzler CC (1970) Phenocryst matrix partition coefficients for K, Rb, Sr and Ba, with application to anorthosite and basalt genesis. Geochim. Cosmochim. Acta 34:307–322

Price RC, Chappell BW (1975) Fractional crystallization and the petrology of Dunedin Volcano. Contrib Mineral Petrol 53:157–182

Reyerson FJ, Hess PC (1978) Implications of liquid-liquid distribution coefficients to mineral-liquid partitioning. Geochim Cosmochim Acta 42:921–932

Ribbe PH (1980) Titanite. In: Orthosilicates Ribbe PH (ed), Min Soc Am, Reviews in Mineralogy 5, pp 137–152

Ringwood AE (1955a) The principles governing trace element distribution during magmatic crystallization. Part I: The influence of electronegativity. Geochim Cosmochim Acta 7:189–202

Ringwood AE (1955b) The principles governing trace element distribution during magmatic crystallization. Part II: The role of complex formation. Geochim Cosmochim Acta 7:242–254

Ritchie GL (1980) Divergent magmas at Crater Lake, Oregon: Products of fractional crystallization and vertical zoning in a shallow, water undersaturatd chamber. J Volcanol Geotherm Res 7:373–386

Schmincke HU (1969a) Ignimbrite sequence on Gran Canaria. Bull Volcanol 33:1199–1219

Schmincke HU (1969b) Petrologie der phonolithischen bis rhyolitischen Vulkanite auf Gran Canaria, Kanarische Inseln. Habilitationsschrift, Ruprecht-Karl Universität Heidelberg, pp 1–151

Schmincke HU (1976) The Geology of the Canary Islands. In: Kunkel G (ed) Biogeography and ecology in the Canary Islands, pp 67–184. The Hague: Junk W. Publishers

Schmincke HU (1977) Eifel Vulkanismus östlich des Gebietes Rieden-Mayen. Fortschr Mineral 55, Bh2, 1–32

Schmincke HU (1982) Vulkane und ihre Wurzeln. Rhein Westf Akad der Wissensch Vorträge N 315, Westdeutscher Verlag, pp 35–78

Schmincke HU, Mertes H (1979) Pliocene and Quaternary volcanic phases in the Eifel volcanic fields. Naturwissensch 66:615–616

Schmincke HU, Lorenz V, Seck HA (1983) Quaternary Eifel volcanic fields. In: Fuchs et al. (ed) Plateau Uplift. The Rhenish Shield – a case history. Heidelberg: Springer, 139–151

Schnetzler CC, Philpotts JA (1970) Partition coefficients of rare earth-elements between igneous matrix material and rock-forming mineral phenocrysts II. Geochim Cosmochim Acta 34:331–340

Schock HH (1977) Trace element partitioning between phenocrysts of plagioclase, pyroxene and magnetite and the host pyroclastic matrix. J Radioanal Chem 38:327–340

Shimizu N (1974) An experimental study of the partitioning of K, Rb, Cs, Sr and Ba between clinopyroxene and liquid at high pressures. Geochim Cosmochim Acta 38:1789–1798

Smith RL (1979) Ash-Flow Magmatism. In: Chapin CE, Elston WE (eds) Ash-Flow Tuffs, pp 5–27. Geol Soc Am Spec Pap 180

Sun SS, Hanson GN (1976) Rare earth evidence for differentiation of McMurdo volcanics. Ross Island, Antarctica. Contrib Mineral Petrol 54:139–155

Watson EB (1976) Two-liquid partition coefficients: Experimental data and geochemical implications. Contrib Mineral Petrol 56:119–134

Watson EB (1977) Partitioning of manganese between forsterite and silicate liquid. Geochim Cosmochim Acta 41:1363–1374

Watson EB (1979) Zircon saturation in felsic liquids, experimental results and applications to trace element geochemistry. Contrib Mineral Petrol 70:407–419

Wörner G (1982) Geochemisch-mineralogische Entwicklung der Laacher See Magmakammer. PhD Thesis Ruhr Universität Bochum, pp 1–331

Wörner G, Schmincke H-U (1984) Mineralogical and chemical zonation of the Laacher See tephra sequence (Germany). J Petrol, in press

Received May 20, 1983; Accepted July 25, 1983